
Swing-Up and Stabilization of a Cart Pendulum System and Stabilization of a Twin Pendulum System

Using Nonlinear Control Strategies

Master Thesis

Aalborg University
Control & Automation
Fredrik Bajers Vej 7
DK-9220 Aalborg

by
Niels Skov Vestergaard



Master Thesis

Control and Automation

Department of Electronic Systems

Fredrik Bajers Vej 7C

9220 Aalborg

Synopsis:

Title:

Swing-Up and Stabilization of a Cart Pendulum System and Stabilization of a Twin Pendulum System

Subtitle:

Using Nonlinear Control Strategies

Theme:

Nonlinear Control

Project Period:

Autumn 2018

Participants:

Niels Skov Vestergaard

Supervisor:

John-Josef Leth

Pages: ?

Appendices: ?

Attachments: ?

Concluded: 2019-01-16

Nam dui ligula, fringilla a, euismod sodales, sollicitudin vel, wisi. Morbi auctor lorem non justo. Nam lacus libero, pretium at, lobortis vitae, ultricies et, tellus. Donec aliquet, tortor sed accumsan bibendum, erat ligula aliquet magna, vitae ornare odio metus a mi. Morbi ac orci et nisl hendrerit mollis. Suspendisse ut massa. Cras nec ante. Pellentesque a nulla. Cum sociis natoque penatibus et magnis dis parturient montes, nascetur ridiculus mus. Aliquam tincidunt urna. Nulla ullamcorper vestibulum turpis. Pellentesque cursus luctus mauris.

Nam dui ligula, fringilla a, euismod sodales, sollicitudin vel, wisi. Morbi auctor lorem non justo. Nam lacus libero, pretium at, lobortis vitae, ultricies et, tellus. Donec aliquet, tortor sed accumsan bibendum, erat ligula aliquet magna, vitae ornare odio metus a mi. Morbi ac orci et nisl hendrerit mollis. Suspendisse ut massa. Cras nec ante. Pellentesque a nulla. Cum sociis natoque penatibus et magnis dis parturient montes, nascetur ridiculus mus. Aliquam tincidunt urna. Nulla ullamcorper vestibulum turpis. Pellentesque cursus luctus mauris.

Publication of this report's contents (including citation) without permission from the authors is prohibited

Contents

1	Introduction	1
Part I Cart Pendulum		2
2	System and Model	3
2.1	System	3
2.2	Model	5
3	Swing-Up Design	8
3.1	Energy Control	9
3.2	Sign-Based Energy Control	16
3.3	Sat-Based Energy Control	17
3.4	Cart Position and Velocity Control	19
4	Stabilization	23
Part II Twin Pendulum		31
5	System and Model	32
5.1	System Addition	32
5.2	Model	32
Appendix		36

1 | Introduction

This project is concerned with developing nonlinear control strategies for a cart pendulum system and to apply these to the set-up provided in the Control and Automation Lab at Aalborg University (AAU).

The project is two part. The objective of the first part is to design a swing-up controller along with a stabilizing controller to catch the pendulum at the upright position.

In the second part an additional pendulum is attached to the cart in the setup making it a twin pendulum system. The idea is to estimate the additional state and ultimately stabilize the two pendulums in upright position.

Part I

Cart Pendulum

2 | System and Model

A brief overview of the relevant system for *Part 1* is presented in this chapter along with a model of the system.

2.1 System

A setup is provided by the Control and Automation Department at AAU, see Figure 2.1.

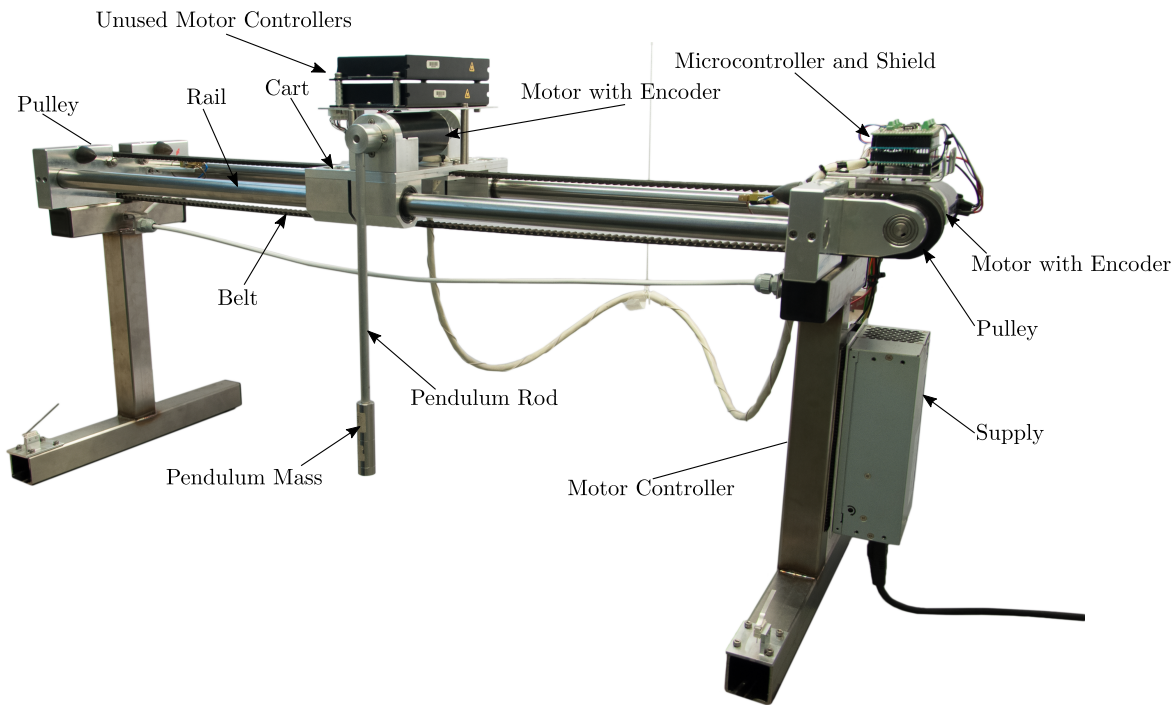


Figure 2.1: The setup provided by AAU. The motor controller in use is not directly visible in this picture as it is mounted behind the power supply.

As seen in Figure 2.1 the belt is attracted by pulleys one of which is driven by a brushed Maxon 370356 DC motor [1]. An other of these maxon motors is mounted on the pendulum but is disconnected and just used as a bearing in this project. Both motors are fitted with an HEDS 5540 optical quadrature encoder allowing for relative position and angle of the cart and pendulum respectively [2].

The motor driving the belt is controlled using a Maxon ADS 50/10 motor controller configured in current control mode. The motor controller takes a $\pm 10\text{ V}$ input signal which then determines the armature current, i_a , see [3].

The primary control unit is a Teensy 3.6 microcontroller board. To program the board

through the onboard USB connection a bootloader is used along with the Teensyduino add-on for the Arduino IDE [4].

The encoders are decoded on a shield using Avago HCTL-2021-PLC decoders and read through an 8 bit parallel data bus on the microcontroller board resulting in 2000 tics pr. revolution. This ensures a resolution for the pendulum angle, θ , of $2\pi/2000 = \pi \times 10^{-3}$ rad/tic and $2\pi r/2000 = 2\pi \cdot 0.028/2000 \approx 0.088 \times 10^{-3}$ m/tic for the cart position, x , see [5].

The supply circuit on the microcontroller board is powered by 5V which is regulated to 3.3 V resulting in a 0–3.3 V range for the 12 bit analog output [6]. This output is used to provide the motor controller with an armature current reference, thus, the microcontroller analog output is amplified through the shield to meet the ± 10 V input requirement of the motor controller [7].

The following relation between analog 12 bit output values, bit_{DAC} , from the microcontroller and armature current in the motor was found by a previous project group [7],

$$\text{bit}_{\text{DAC}} = 105.78 \cdot i_a + 1970 , \quad (2.1)$$

and as a result of a force test, see [8], Equation 2.1 was corrected to,

$$\text{bit}_{\text{DAC}} = 111.9 \cdot i_a + 1970 , \quad (2.2)$$

which is the relation used in this project. All the system parameters used in the design are listed in Table 2.1. It is assumed that all frictions in the system can be modeled as a combination of Coulomb and viscous frictions. Wires hanging from the cart are unmodeled and their weight along with that of the belt are contained in the estimation of the cart mass.

Parameter	Notation	Quantity	Unit
Nominal current (max. continuous current)	I_N	4.58	A
Torque constant	τ_m	93.4×10^{-3}	$\text{N} \cdot \text{m} \cdot \text{A}^{-1}$
Rod Length	l	0.3235	m
Rail Length	l_r	0.89	m
Pulley Radius	r	0.028	m
Pendulum Mass	m	0.201	kg
Cart Mass	M	5.273	kg
Cart Coulomb Friction	$b_{c,c}$	2.884	N
Cart Viscous Friction	$b_{c,v}$	1.680	$\text{N} \cdot \text{m}^{-1} \cdot \text{s}$
Pendulum Coulomb Friction	$b_{p,c}$	0.004	N·m
Pendulum Viscous Friction	$b_{p,v}$	0.4×10^{-3}	$\text{N} \cdot \text{m} \cdot \text{s}$

Table 2.1: The motor parameters, I_N and τ_m , are given by maxon in [1]. The rod length is measured from the pendulum pivot point to the geometrical center of the pendulum. Pendulum mass, rod length, pulley radius and rail length are measured parameters, while cart mass is estimated same as all frictions. The estimations are performed by a previous project group [7].

2.2 Model

The model is based on the generalized coordinates presented in Figure 2.2.

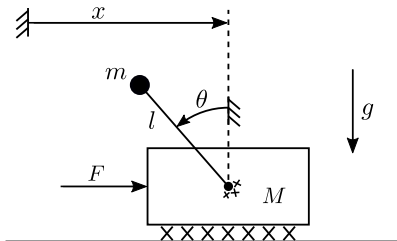


Figure 2.2: Mechanical drawing of the system, where θ is the angle of the pendulum, x is the position of the center of the cart along the rail, F is the applied force and g is the gravitational acceleration. It is indicated that friction is modeled between cart and rail as well as in the pendulum joint.

The pendulum mass center is positioned at zero height at rest s.t. all energies in the system are positive. It is assumed that the pendulum rod is rigid and massless and that the pendulum weights are a point mass at the geometrical center of the weights.

The motor torque is given by direct relation to the armature current by the motor constant, $\tau_m = k_\tau i_a$, such that,

$$F = \frac{1}{r} k_\tau i_a \quad . \quad (2.3)$$

To avoid excessive notation $u = F$ is considered to be the control input in the remaining of this thesis, while keeping in mind the relation in Equation 2.3 along with the knowledge that u must be converted to armature current in implementation.

It is well known that the potential energy, U , and the kinetic energy, T , are given by, [9]

$$U = mgl(1 + \cos \theta) \quad (2.4)$$

$$T = \frac{1}{2}(M + m)\dot{x}^2 - ml\cos\theta\dot{\theta} + \frac{1}{2}ml^2\dot{\theta}^2 \quad . \quad (2.5)$$

The frictions, indicated in Figure 2.2, are, as mentioned, comprised of Coulomb and viscous frictions with values stated in Table 2.1. The viscous frictions are modeled as linear functions of velocities, [10, 11]

$$b_{p,v}\dot{\theta} \quad , \quad b_{c,v}\dot{x} \quad , \quad (2.6)$$

for the rotational and linear case respectively. The coulomb frictions are modeled as a constant with its sign depending on the signs of the velocities, such that, [10, 11]

$$\operatorname{sgn}(\dot{\theta})b_{p,c} \quad , \quad \operatorname{sgn}(\dot{x})b_{c,c} \quad . \quad (2.7)$$

This, however, introduces discontinuities at zero velocities. Thus, tanh-functions are used to obtain a continues approximation of the sign-functions,

$$\tanh(k_{\tanh}\dot{\theta})b_{p,c} \quad , \quad b_{c,v}\dot{x} - \tanh(k_{\tanh}\dot{x})b_{c,c} \quad , \quad (2.8)$$

where $k_{\tanh} = 250$ to increase the steepness of the tanh-functions thereby obtaining a closer approximation of the sign-functions. Finally, by use of the Lagrange-d'Alembert Principle, [9]

$$\frac{d}{dt} \frac{\partial \mathcal{L}}{\partial \dot{\mathbf{q}}} - \frac{\partial \mathcal{L}}{\partial \mathbf{q}} = \mathbf{Q} \quad , \quad (2.9)$$

$$\mathbf{q} = \begin{bmatrix} \theta \\ x \end{bmatrix} \quad , \quad \mathbf{Q} = \begin{bmatrix} -b_{p,v}\dot{\theta} - \tanh(k_{\tanh}\dot{\theta})b_{p,c} \\ \frac{1}{r}k_{\tau}i_a - b_{c,v}\dot{x} - \tanh(k_{\tanh}\dot{x})b_{c,c} \end{bmatrix} \quad , \quad (2.10)$$

and $\mathcal{L} = \mathcal{T} - \mathcal{U}$, the dynamics of the system are found,

$$ml^2\ddot{\theta} - ml\cos\theta\ddot{x} - mgl\sin\theta = -b_{p,v}\dot{\theta} - \tanh(k_{\tanh}\dot{\theta})b_{p,c} \quad (2.11)$$

$$(M + m)\ddot{x} + ml\sin\theta\dot{\theta}^2 - ml\cos\theta\ddot{\theta} = u - b_{c,v}\dot{x} - \tanh(k_{\tanh}\dot{x})b_{c,c} \quad . \quad (2.12)$$

By setting up the dynamic equations, Equation 2.12 and 2.11, in the following manner,

$$\begin{bmatrix} ml^2 & -ml\cos\theta \\ -ml\cos\theta & M + m \end{bmatrix} \begin{bmatrix} \ddot{\theta} \\ \ddot{x} \end{bmatrix} + \begin{bmatrix} 0 \\ ml\sin\theta\dot{\theta}^2 \end{bmatrix} + \begin{bmatrix} b_{p,v}\dot{\theta} + \tanh(k_{\tanh}\dot{\theta})b_{p,c} \\ b_{c,v}\dot{x} + \tanh(k_{\tanh}\dot{x})b_{c,c} \end{bmatrix} + \begin{bmatrix} -mgl\sin\theta \\ 0 \end{bmatrix} = \begin{bmatrix} 0 \\ u \end{bmatrix} \quad , \quad (2.13)$$

Chapter 2. System and Model

the general form of an m-link robot is obtained, [12, 13]

$$\mathbf{M}(\mathbf{q})\ddot{\mathbf{q}} + \mathbf{C}(\mathbf{q}, \dot{\mathbf{q}}) + \mathbf{B}(\dot{\mathbf{q}}) + \mathbf{G}(\mathbf{q}) = \mathbf{F} \quad , \quad (2.14)$$

where,

$\mathbf{M}(\mathbf{q})$ is the inertia matrix

$\mathbf{C}(\mathbf{q}, \dot{\mathbf{q}})$ is the Coriolis and centrifugal effects

$\mathbf{B}(\dot{\mathbf{q}})$ is the friction

$\mathbf{G}(\mathbf{q})$ is the force due to gravity

\mathbf{F} is the input force vector .

Choosing $[x_1 \ x_2 \ x_3 \ x_4]^T = [\theta \ x \ \dot{\theta} \ \dot{x}]^T$ as states results in the following nonlinear state space representation,

$$\begin{bmatrix} \dot{x}_1 \\ \dot{x}_2 \\ \dot{x}_3 \\ \dot{x}_4 \end{bmatrix} = \begin{bmatrix} & & x_3 \\ & & x_4 \\ & & \\ \mathbf{M}^{-1}(x_1)(\mathbf{F} - \mathbf{C}(x_1, x_3) - \mathbf{B}(x_3, x_4) - \mathbf{G}(x_1)) \end{bmatrix} , \quad (2.15)$$

which is convenient when simulating the system. This representation is also used in the controller designs.

3 | Swing-Up Design

In this chapter three swing-up controllers are designed, all based on [14]. The pendulum is started at rest, $\theta = \pi$, with the angle convention specified in Figure 2.2. The idea of the swing-up controller is to increase the mechanical energy in the system until it matches that of the desired end state, $\theta = 0$ and $\dot{\theta} = 0$, that is, the upright position at rest. The minimum energy in the system occurs at the starting position at rest, which is considered to be zero as mentioned in the *Model* section 2.2. So the target energy is $E_{\text{eq}} = 2mgl$, that is, the potential energy of the pendulum in the unstable equilibrium.

Consider the pendulum dynamics from Equation 2.12, where $J = ml^2$ is the pendulum inertia and frictions are assumed to be zero such that,

$$J\ddot{\theta} - ml \cos \theta a_c - mgl \sin \theta = 0 \quad . \quad (3.1)$$

This equation captures the behavior of the pendulum corresponding to some controlled acceleration a_c at the pivot point. This acceleration is viewed as the control input for now. The force needed to achieve this acceleration is considered at the end of the design. It is further convenient to describe the energy of the pendulum with the coordinate frame fixed at its pivot point, see Figure 3.1.

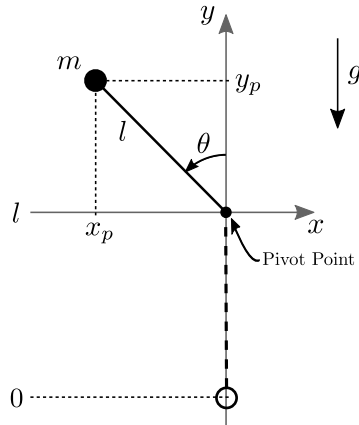


Figure 3.1: The energy used in the swing-up controller is described using this convention, where the coordinate frame is fixed at the pivot point of the pendulum. The zero reference is placed as before s.t. all energies are positive.

From Figure 3.1, the conversion from excessive to generalized coordinates is given by,

$$x_p = -l \sin \theta \quad , \quad y_p = l(\cos \theta + 1) \quad , \quad \dot{x}_p = -l \cos \theta \dot{\theta} \quad , \quad \dot{y}_p = -l \sin \theta \dot{\theta} \quad . \quad (3.2)$$

The mechanical energy in this coordinate frame is then,

$$E_p = mgy_p + \frac{1}{2}m\dot{x}_p^2 + \frac{1}{2}m\dot{y}_p^2 \quad (3.3)$$

$$E_p = mgl(\cos \theta + 1) + \frac{1}{2}m(-l \cos \theta \dot{\theta})^2 + \frac{1}{2}m(-l \sin \theta \dot{\theta})^2 \quad (3.4)$$

$$E_p = mgl(\cos \theta + 1) + \frac{1}{2}J(\cos^2 \theta + \sin^2 \theta)\dot{\theta}^2 \quad (3.5)$$

$$E_p = \frac{1}{2}J\dot{\theta}^2 + mgl(\cos \theta + 1) \quad . \quad (3.6)$$

The following sections explores different approaches of controlling the pendulum energy specified in Equation 3.6 to its desired reference.

3.1 Energy Control

A function candidate is proposed,

$$V(\theta, \dot{\theta}) = \frac{1}{2}E_{\Delta}^2 \quad , \quad (3.7)$$

where E_{Δ} is the difference in energy in relation to the unstable equilibrium,

$$E_{\Delta} = E_p - E_{\text{eq}} \quad (3.8)$$

$$E_{\Delta} = \frac{1}{2}J\dot{\theta}^2 + mgl(\cos \theta + 1) - 2mgl \quad (3.9)$$

$$E_{\Delta} = \frac{1}{2}J\dot{\theta}^2 + mgl(\cos \theta - 1) \quad , \quad (3.10)$$

hence,

$$V = \frac{1}{2}(\frac{1}{2}J\dot{\theta}^2 + mgl(\cos \theta - 1))^2 \quad (3.11)$$

$$V = \frac{1}{2}(\frac{1}{2}J\dot{\theta}^2)^2 + \frac{1}{2}(mgl(\cos \theta - 1))^2 + \frac{1}{2}J\dot{\theta}^2mgl(\cos \theta - 1) \quad (3.12)$$

$$V = \frac{1}{8}J^2\dot{\theta}^4 + \frac{1}{2}m^2g^2l^2(\cos^2 \theta + 1 - 2 \cos \theta) + \frac{1}{2}J\dot{\theta}^2mgl(\cos \theta - 1) \quad , \quad (3.13)$$

further,

$$\frac{\partial V}{\partial \theta} = -m^2g^2l^2 \cos \theta \sin \theta + m^2g^2l^2 \sin \theta - \frac{1}{2}J\dot{\theta}^2mgl \sin \theta \quad (3.14)$$

$$\frac{\partial V}{\partial \dot{\theta}} = \frac{1}{2}J^2\dot{\theta}^3 + Jmgl(\cos \theta - 1)\dot{\theta} \quad , \quad (3.15)$$

where both Equation 3.14 and 3.15 are continuous, C^0 , so $V(\theta, \dot{\theta})$ is continuously differentiable, C^1 , in the entire \mathbb{R}^2 .

The idea is to reach the reference $E_{\Delta} = 0$, which happens when,

$$\frac{1}{2}J\dot{\theta}^2 + mgl(\cos \theta - 1) = 0 \quad (3.16)$$

$$\dot{\theta} = \pm \left(\frac{-2mgl(\cos \theta - 1)}{J} \right)^{\frac{1}{2}} \quad . \quad (3.17)$$

A plot of Equation 3.17 in the phase plane, see Figure 3.2, reveals a set of solutions joining the two unstable equilibrium points.

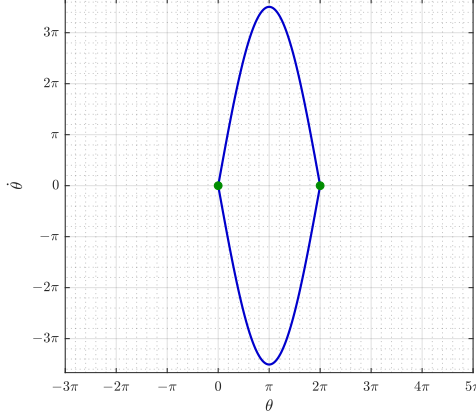


Figure 3.2: If the trajectories of the system are restricted to this set, the energy error is maintained at zero and the trajectories form a heteroclinic orbit.

If the energy reference is successfully tracked, the system will be restricted to this set rather than a single equilibrium point. Such a trajectory joining two equilibrium points is called a heteroclinic orbit.

Recall the system from Equation 3.1,

$$J\ddot{\theta} = ml \cos \theta a_c + mgl \sin \theta , \quad (3.18)$$

the derivative of V is then evaluated along trajectories of the system,

$$\dot{V} = E_\Delta \dot{E}_\Delta \quad (3.19)$$

$$\dot{V} = E_\Delta (J\dot{\theta}\ddot{\theta} - mgl \sin \theta \dot{\theta}) \quad (3.20)$$

$$\dot{V} = E_\Delta (\dot{\theta}(ml \cos \theta a_c + mgl \sin \theta) - mgl \sin \theta \dot{\theta}) \quad (3.21)$$

$$\dot{V} = ml E_\Delta \cos \theta \dot{\theta} a_c . \quad (3.22)$$

The idea is to find a control law, a_c , which allows trajectories of the system to reach the desired heteroclinic orbit. By studying LaSalle's Theorem 3.1.1, analysis of convergence to sets is made possible.

Theorem 3.1.1 (LaSalle's Theorem) Consider the autonomous system, $f(\mathbf{x}) = \dot{\mathbf{x}}$, where $f : \mathbb{D} \rightarrow \mathbb{R}^n$ is locally Lipschitz and $\mathbf{x} = \mathbf{0}$ is an equilibrium point. Then if there exist some function $V : \mathbb{D} \rightarrow \mathbb{R}$ and

1. $V(\mathbf{x})$ is C^1
2. $\exists c > 0$ s.t. $\Omega_c = \{\mathbf{x} \in \mathbb{R}^n \mid V(\mathbf{x}) \leq c\} \subset \mathbb{D}$ is bounded
3. $\dot{V}(\mathbf{x}) \leq 0 \quad \forall \mathbf{x} \in \Omega_c$

then $\mathbf{x}(0) \in \Omega_c \Rightarrow \mathbf{x}(t) \xrightarrow{t \rightarrow \infty} M$, where M is the largest invariant set in

$$E = \{\mathbf{x} \in \Omega_c \mid \dot{V}(\mathbf{x}) = 0\} \quad [15].$$

Chapter 3. Swing-Up Design

The first condition in LaSalle's Theorem 3.1.1 is already satisfied. Notice that the function candidate, $V(\mathbf{x})$, is not required to be positive definite.

The second condition states that some bounded set, Ω_c , of solutions for which $V(\mathbf{x})$ is less than or equal to some constant c must exist.

This ties into the third condition stating that the derivative of the function candidate must be negative semi-definite along trajectories of the system for all solutions in said set. The controlled acceleration at the pivot point, a_c , is then designed to satisfy the third condition in Theorem 3.1.1,

$$a_c = -kE_\Delta \cos \theta \dot{\theta} \quad , \quad (3.23)$$

where the tuning parameter, $k > 0$, is introduced to allow scaling the control output to fit the capabilities of the actuator. Inserting the control law yields,

$$\dot{V} = mE_\Delta \cos \theta \dot{\theta}(-kE_\Delta \cos \theta \dot{\theta}) \quad (3.24)$$

$$\dot{V} = -kml(E_\Delta \cos \theta \dot{\theta})^2 \leq 0 \quad , \quad (3.25)$$

satisfying the third condition of Theorem 3.1.1 not only in Ω_c but in the entire state space. This means any $\infty > c > 0$ will satisfy the second condition. However, looking at the function candidate,

$$V = \frac{1}{8}J^2\dot{\theta}^4 + \frac{1}{2}m^2g^2l^2(\cos^2 \theta + 1 - 2\cos \theta) + \frac{1}{2}J\dot{\theta}^2mgl(\cos \theta - 1) \quad , \quad (3.26)$$

the angle is only present in periodic functions. Hence no value of c can bound the angle. If starting some arbitrary place in the state space, the energy reference is eventually tracked, but the heteroclinic orbit could settle between any two saddle points. To constrain further analysis and design to the desired region of operation, Ω_c is defined as the set containing all points within and on the set in Figure 3.2, that is,

$$\Omega_c = \{\mathbf{x} \mid \dot{\theta} \leq \left(\frac{-2mgl(\cos \theta - 1)}{J} \right)^{\frac{1}{2}}, 0 \leq \theta \leq 2\pi\} \quad . \quad (3.27)$$

All conditions of LaSalle's Theorem 3.1.1 are satisfied, thus, if starting in Ω_c , trajectories of the system will converge to M as time goes to infinity. M is the largest invariant set in E , which can be described as the union of sets for which Equation 3.25 is zero,

$$A = \{\mathbf{x} \in \Omega_c \mid E_\Delta = 0\} \quad (3.28)$$

$$B = \{\mathbf{x} \in \Omega_c \mid \cos \theta = 0\} \quad (3.29)$$

$$C = \{\mathbf{x} \in \Omega_c \mid \dot{\theta} = 0\} \quad (3.30)$$

$$E = A \cup B \cup C \quad . \quad (3.31)$$

To construct set M it is necessary to evaluate each set for invariance with respect to the controlled system. A proof is developed to show invariance of set A . Recall the relation between $\dot{\theta}$ and θ for $E_\Delta = 0$,

$$\dot{\theta}_z = \pm \left(\frac{-2mgl(\cos \theta - 1)}{J} \right)^{\frac{1}{2}} \quad , \quad (3.32)$$

where $\dot{\theta}_z$ is the angular velocity for which the energy error is zero. Further, consider the controlled system in following form,

$$\ddot{\theta} = \frac{1}{J}(-kml \cos \theta E_{\Delta} \cos \theta \dot{\theta} + mgl \sin \theta) \quad . \quad (3.33)$$

To prove that A is invariant with respect to Equation 3.33, the slope of $\dot{\theta}_z$ is compared to the slope of the controlled system trajectories in the set. If the slopes are equal, then no trajectory can leave the set A , thus proving A is invariant with respect to the controlled system. The slope of $\dot{\theta}_z$ is,

$$\frac{\partial \dot{\theta}_z}{\partial \theta} = \pm \frac{mgl \sin \theta}{J} \left(\frac{-2mgl(\cos \theta - 1)}{J} \right)^{-\frac{1}{2}} \quad (3.34)$$

$$\frac{\partial \dot{\theta}_z}{\partial \theta} = \frac{mgl \sin \theta}{J \dot{\theta}_z} \quad . \quad (3.35)$$

The slope of the trajectories of the controlled system, Equation 3.33, in set A is then,

$$b = \frac{\ddot{\theta}_z}{\dot{\theta}_z} \quad (3.36)$$

$$b = \frac{-kml \cos^2 \theta E_{\Delta}(\theta, \dot{\theta}_z) \dot{\theta}_z + mgl \sin \theta}{J \dot{\theta}_z} \quad (3.37)$$

$$b = \frac{-kml \cos^2 \theta (\frac{1}{2} J \dot{\theta}_z^2 + mgl(\cos \theta - 1)) \dot{\theta}_z + mgl \sin \theta}{J \dot{\theta}_z} \quad (3.38)$$

$$b = -kml \cos^2 \theta \frac{1}{2} \dot{\theta}_z^2 - \frac{1}{J} kml \cos^2 \theta mgl(\cos \theta - 1) + \frac{mgl \sin \theta}{J \dot{\theta}_z} \quad (3.39)$$

$$b = -kml \cos^2 \theta \frac{1}{2} \left(\frac{-2mgl(\cos \theta - 1)}{J} \right) - \frac{1}{l^2 m} km^2 l^2 g \cos^2 \theta (\cos \theta - 1) + \frac{mgl \sin \theta}{J \dot{\theta}_z} \quad (3.40)$$

$$b = -kml \cos^2 \theta \frac{1}{2} \frac{-2mgl(\cos \theta - 1)}{l^2 m} - k \cos^2 \theta mg(\cos \theta - 1) + \frac{mgl \sin \theta}{J \dot{\theta}_z} \quad (3.41)$$

$$b = k \cos^2 \theta mg(\cos \theta - 1) - k \cos^2 \theta mg(\cos \theta - 1) + \frac{mgl \sin \theta}{J \dot{\theta}_z} \quad (3.42)$$

$$b = \frac{mgl \sin \theta}{J \dot{\theta}_z} \quad , \quad (3.43)$$

where $\ddot{\theta}_z$ is the angular acceleration of the controlled system in set A .

Finally, since,

$$\frac{\partial \dot{\theta}_z}{\partial \theta} = b \quad , \quad (3.44)$$

the set A is invariant with respect to the controlled system. The set B is invariant only for the intersection $B \cap A$, any other values of the angular velocity will cause it to leave the set since $\cos \theta = 0$ corresponds to a horizontal position of the pendulum. A similar

Chapter 3. Swing-Up Design

argument can be made for set C , however, in this case if $\theta = \pi$, the system stays in the set. So, the invariant part of set C excluding A is,

$$F = \{\mathbf{x} \in \Omega_c \mid \dot{\theta} = 0, \theta = \pi\}, \quad (3.45)$$

thus the largest invariant set in E is,

$$M = A \cup F. \quad (3.46)$$

The sets are visualized in Figure 3.3.

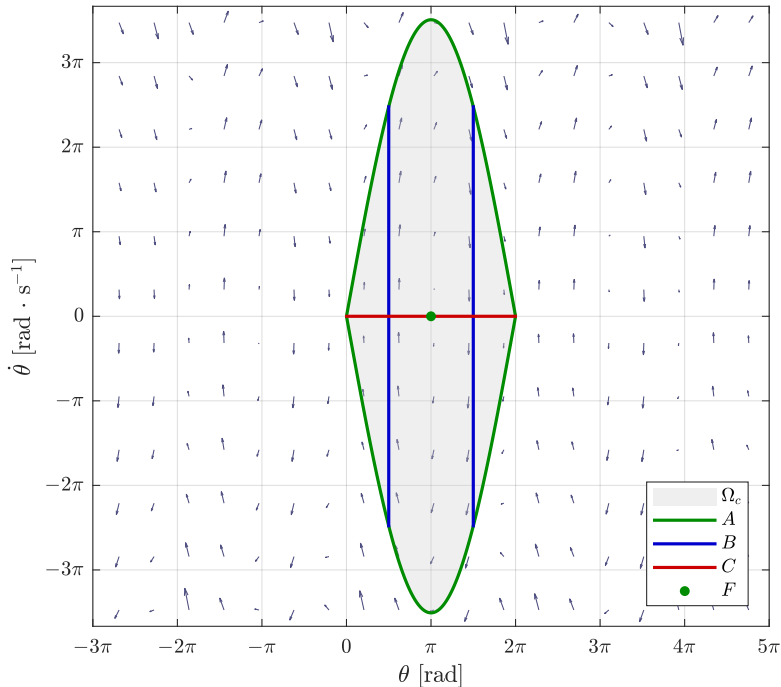


Figure 3.3: The set Ω_c shown along with sets in Ω_c for which $\dot{V}(\mathbf{x}) = 0$. Set A and F together form the largest invariant set M in E . The phase portrait of the controlled system shows how its trajectories line up with A indicating invariance of A with respect to the controlled system.

If this control law is started at zero angular velocity, $\dot{\theta} = 0$, in the stable equilibrium, the computed control is maintained at zero and the pendulum never swings up. So for this control law to work, the pendulum must be started slightly away from the stable equilibrium.

An extra step is needed to apply this control strategy. So far the control output is an acceleration, a_c , at the pivot point. It is possible to input the desired acceleration, a_c , into the second dynamic equation, Equation 2.12, and solve for the force needed to achieve this acceleration,

$$u = (M + m)a_c + ml \sin x_1 x_3^2 - ml \cos x_1 \dot{x}_3, \quad (3.47)$$

where the cart friction coefficients are set to zero again.

To calculate the force from this expression, Equation 3.47, it is also necessary to know the angular acceleration of the pendulum, \dot{x}_3 , which can be solved for in the system dynamics, Equation 2.15, inserting known states and control input applied in the previous step,

$$\begin{bmatrix} \dot{x}_3 \\ \dot{x}_4 \end{bmatrix} = \begin{bmatrix} ml^2 & -ml \cos x_1 \\ -ml \cos x_1 & M+m \end{bmatrix}^{-1} \begin{bmatrix} -b_{p,v}x_3 - \tanh(k_{\tanh}x_3)b_{p,c} + mgl \sin x_1 \\ u_{last} - ml \sin x_1 x_3^2 \end{bmatrix}, \quad (3.48)$$

where u_{last} is the force applied in the previous step.

From Equation 3.48 the approximated angular acceleration is then,

$$\dot{x}_3 = \frac{(M+m)(-b_{p,v}x_3 - \tanh(k_{\tanh}x_3)b_{p,c} + mgl \sin x_1)}{l^2m(M+m - m \cos^2 x_1)} + \frac{\cos x_1(u_{last} - ml \sin x_1 x_3^2)}{l(M+m - m \cos^2 x_1)}. \quad (3.49)$$

Inserting Equation 3.49 into Equation 3.47 results in the control input, u , necessary to achieve the desired acceleration, a_c , at the pivot point. This method is used for all three swing-up controllers, so to avoid excessive notation the proceeding energy control laws are derived with a_c as the control parameter.

All simulations are performed using the nonlinear state space representation in Equation 2.15 and the matlab ODE45 solver with a relative tolerance of 1×10^{-7} . Initializing the angle, θ , at $\pi - 0.1$ to avoid zero control output as discussed, the energy difference struggles to reach its reference at zero, see Figure 3.4. The pendulum friction and cart inertia are included in the calculation of the force needed to obtain the desired acceleration. This, however, is not concerned with what is needed to obtain the required energy. So the offset seen in Figure 3.4 is caused by the control law, Equation 3.23, asking for insufficient acceleration.

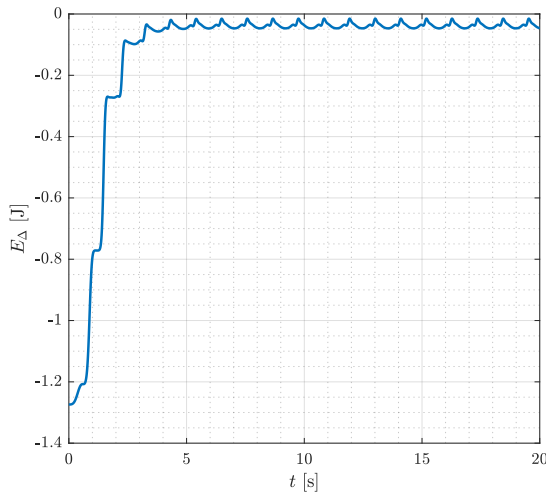


Figure 3.4: Simulation of the first energy control method. The energy error struggles to maintain zero value, due to pendulum friction and cart inertia exchanging energy with the pendulum.

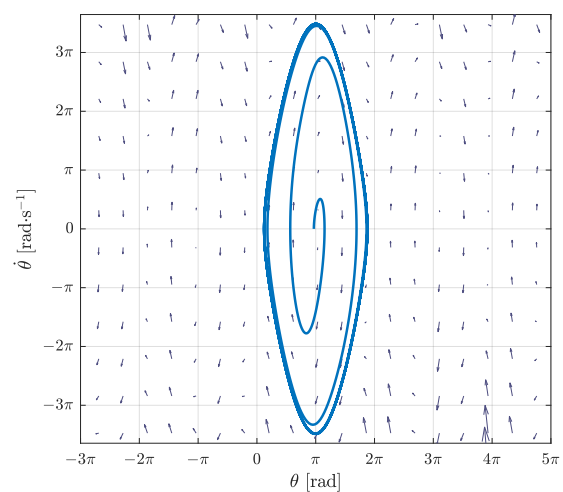


Figure 3.5: This phase portrait shows the attempt to reach the heteroclinic orbit. It falls short due to the insufficient acceleration asked by the control law.

Chapter 3. Swing-Up Design

The pendulum also falls short of reaching the heteroclinic orbit, see Figure 3.5. Further, since the energy of the pendulum is not affected by the position or velocity of the cart, this control law, Equation 3.23, is not concerned with controlling these. This becomes a problem in the physical setup as it has a rail length of 0.89 m, see Table 2.1. A traced animation is used to demonstrate this problem in Figure 3.6.

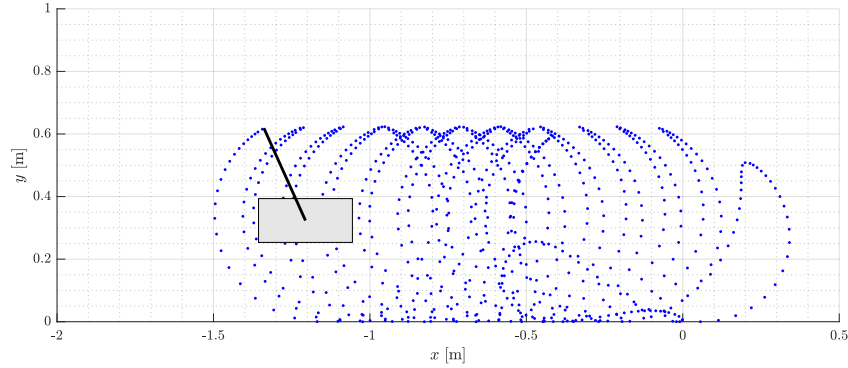


Figure 3.6: The cart drifts beyond the bounds of the physical system. This might not be a problem if the catch controller catches the pendulum in first try, but there is no guarantee of this being the case.

An other issue is the actuation which is limited in the real system by the maximum allowed continuous current, see Table 2.1. By tuning the parameter k in the control law, better performance can be obtained, however at the cost of excessive actuation.

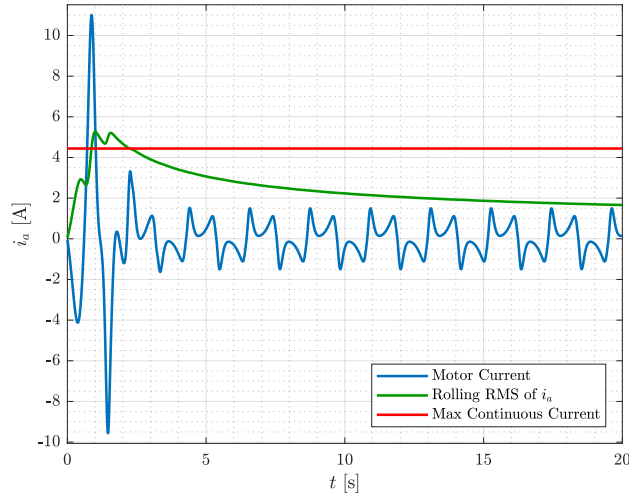


Figure 3.7: The motor current has high peaks in the beginning which likely exceeds the capabilities of the motor. The controller is tuned such that the RMS value of the current does not exceed the maximum continuous current requirement of the motor for a sustained period of time.

For these graphs $k = 1.3$ to keep the motor current at acceptable levels. The motor current is shown in Figure 3.7 where the rolling RMS of i_a is used to approximate the continuous current load on the motor. Though the continuous current is acceptable, the peaks in the start will be saturated in the real system, which would cause a longer rise time for the energy.

3.2 Sign-Based Energy Control

There are other ways to satisfy Equation 3.25 than the control law suggested in Equation 3.23. To achieve maximal actuation a sign-function can be used to determine the direction of actuation along with a gain k to adjust for the limits of the actuator as before,

$$a_c = k \operatorname{sgn}(-E_\Delta \cos \theta \dot{\theta}) , \quad (3.50)$$

where,

$$\operatorname{sgn}(s(\theta, \dot{\theta})) = \begin{cases} 1 & s > 0 \vee \cos \theta \dot{\theta} = 0 \\ 0 & s = 0 \wedge \cos \theta \dot{\theta} \neq 0 \\ -1 & s < 0 \end{cases} , \quad (3.51)$$

to avoid no actuation when starting at stable equilibrium. This adjustment reduces the set,

$$M = \{\mathbf{x} \in \Omega_c \mid E_\Delta = 0\} , \quad (3.52)$$

such that convergence to M when starting in Ω_c , by Theorem 3.1.1, now assures convergence to the energy reference and thus to the heteroclinic orbit.

The gain is tuned to $k = 2.7$ in the following simulation. Looking at the energy in Figure 3.8, this strategy seems to work really well. From the phase portrait in Figure 3.9 it is evident that a near perfect heteroclinic orbit is reached.

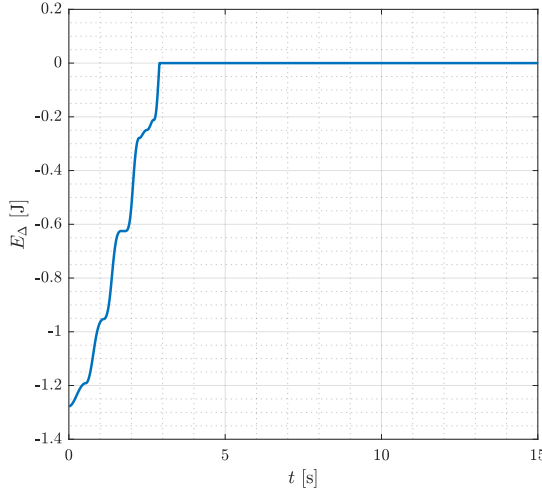


Figure 3.8: Using maximum actuation in the appropriate direction drives the energy error to zero and keeps it there.

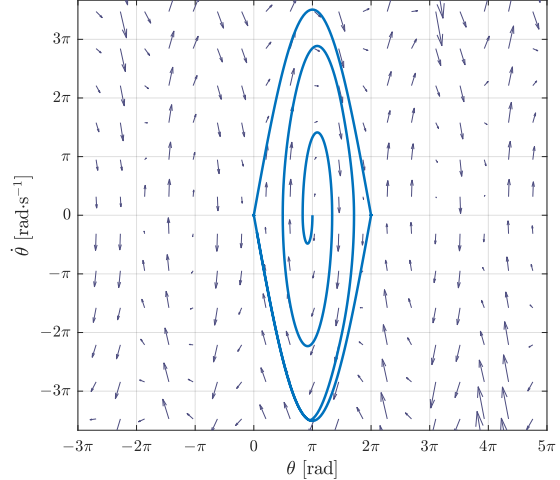


Figure 3.9: The heteroclinic orbit is reached very accurately.

In Figure 3.10 however, while the angle reaches the equilibrium as closely as possible without overshooting, this control law, as with the previous, does not account for position of the cart.

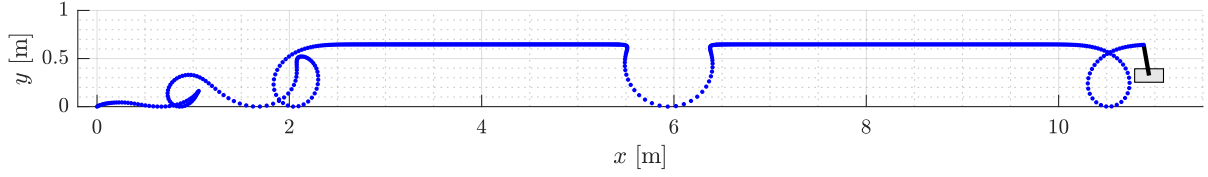


Figure 3.10: The cart drifts as before, since the controller is only concerned with the energy of the pendulum.

However, the bigger problem with this control law is obvious from Figure 3.11, where excessive switching shows on the control output.

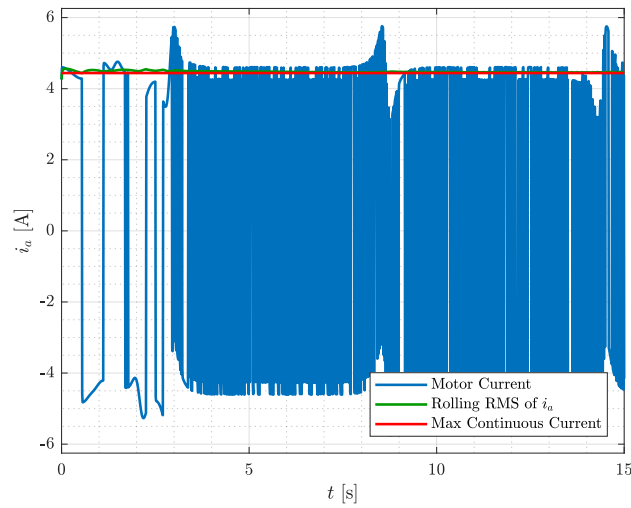


Figure 3.11: The sign-function in the control law causes excessive switching in the output, thus, the design is not feasible for a real system implementation.

This actuation behavior is not feasible in a real system and attempted implementation will cause chattering resulting in unwanted behavior and wear of the motor. In next section it is attempted to solve this issue, while keeping some of the performance of this approach.

3.3 Sat-Based Energy Control

To avoid the excessive switching of the sign-based controller a different strategy using a saturation function is investigated,

$$a_c = \text{sat}(-kE_\Delta \text{sgn}(\cos \theta \dot{\theta})) \quad , \quad (3.53)$$

where

$$\text{sgn}(s) = \begin{cases} 1 & |s| \geq 0 \\ -1 & |s| < 0 \end{cases} \quad , \quad (3.54)$$

and the sat-function saturates at the minimum/maximum allowed acceleration. The known limitation is $i_{max} = 4.58$ as stated in Table 2.1, from which the maximum control, u , can be calculated,

$$u_{max} = \frac{k_\tau}{r} , \quad (3.55)$$

and finally, by disregarding the pendulum behavior and cart friction from the dynamics in Equation 2.12,

$$a_{max} = \frac{u_{max}}{M + m} . \quad (3.56)$$

As this is a crude estimate $0.1 \text{ m} \cdot \text{s}^{-2}$ is subtracted from the estimated a_{max} in following simulations to stay within the actuation limits. The saturation function is then,

$$\text{sat}(s) = \begin{cases} s & |s| \leq a_{max} \\ \text{sgn}(s) a_{max} & |s| > a_{max} \end{cases} . \quad (3.57)$$

Notice how the sgn-function in this control law, Equation 3.53, only takes $\cos \theta \dot{\theta}$ as input. Contrary to the sign-based controller which also included E_Δ causing the need for complicated restrictions in the definition of the sgn-function.

Choice of k decides how aggressive the controller should be. Larger values of k drives the control into saturation faster thus actuating more like the sign-based controller in Equation 3.50. At lower values of k the operation will not reach saturation as fast thus behaving more like the first energy based controller in Equation 3.23. For an effective swing up behavior $k = 200$ is chosen, thus approaching the behavior of the sign-based controller, which makes sense as this is the theoretically ideal solution.

This control strategy achieves the energy reference in about three seconds, Figure 3.12, as is the case of the sign-based strategy, Figure 3.8. Further, from Figure 3.13, the system still reaches a near perfect heteroclinic orbit.

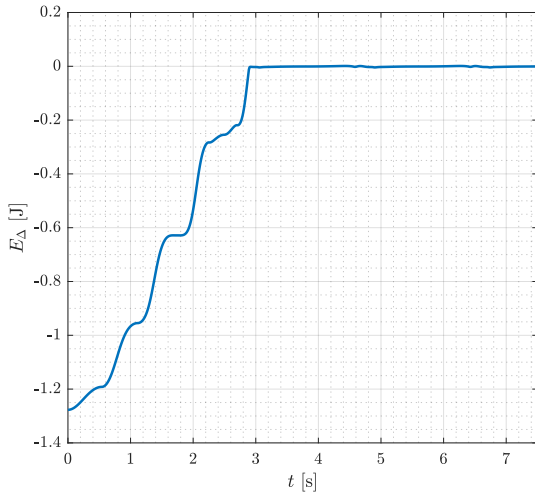


Figure 3.12: The sat-based controller shows no loss in performance when comparing the energy error to that of the sign-based approach.

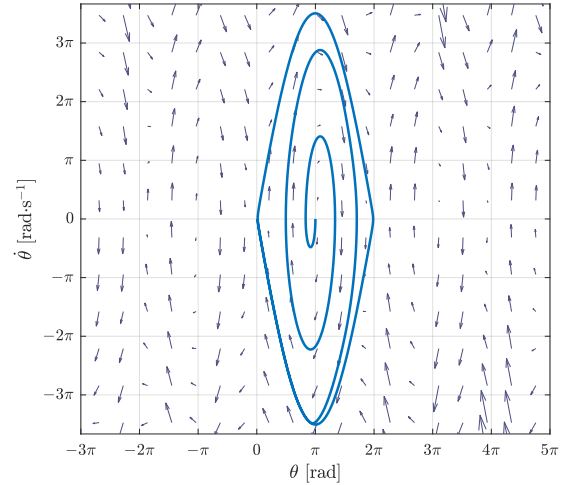


Figure 3.13: The heteroclinic orbit is still reached, however, with a more realistic trajectory at the approach of the equilibrium points.

Chapter 3. Swing-Up Design

The cart still drifts as expected, see Figure 3.14, and the equilibrium points are maintained for shorter duration, which is expected with less control switching. Figure 3.14.

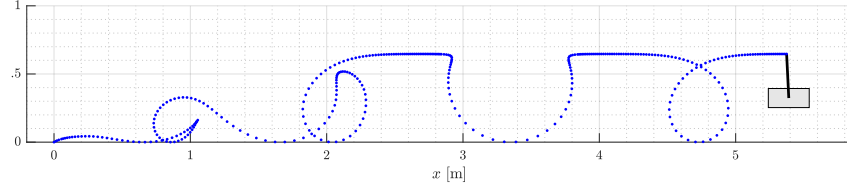


Figure 3.14: This strategy performs well. The drifting problem is solved later.

The excessive switching on the control output is successfully avoided, see Figure 3.15, resulting in a much more realistic control signal compared to that in Figure 3.11.

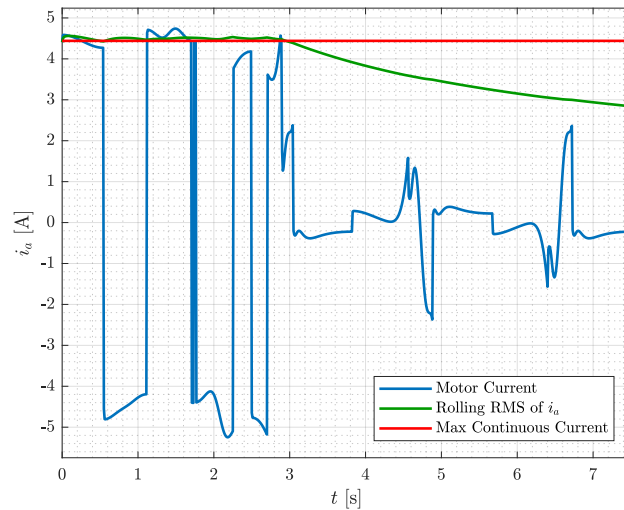


Figure 3.15: The control signal using the sat-based approach is much more realistic for implementation as the excessive switching of the sign-based controller is successfully avoided.

The design of the energy based control law, Equation 3.53, is concluded. The problem of controlling the cart position still remains. In the following, the performance of this control law is subjected to the disturbance caused by added control on the cart position and velocity.

3.4 Cart Position and Velocity Control

To solve the cart drifting problem along x a linear controller is designed and added to the control law,

$$a_c = \psi(x_1, x_3) + v(x_2, x_4) \quad , \quad (3.58)$$

where $\psi(x_1, x_3)$ is the energy controller and $v(x_2, x_4)$ is the linear controller. While these two controllers depend on different states, they still influence and act as unmodeled disturbances to one another. The position and velocity control, $v(x_2, x_4)$, adds and subtracts

energy, therefore could cause the energy controller, $\psi(x_1, x_3)$, to overshoot. One solution to this potential problem could be to slightly lower the energy reference. However, swing-up is often designed with a higher energy reference such that the catch controller has some entry velocity at the unstable equilibrium.

With these considerations in mind, the design of $v(x_2, x_4)$ is proceeded. Considering the cart without friction and assuming any influence of the pendulum dynamics and the energy control to be unmodeled disturbances of the system. This reduces the model to the mechanical drawing seen in Figure 3.16.

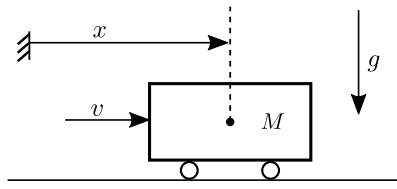


Figure 3.16: Mechanical drawing of the reduced model used for position control.

The dynamics are then,

$$M\ddot{x} = v \quad , \quad (3.59)$$

and selecting new states $[z_1 \ z_2]^T = [x \ \dot{x}]^T$, the linear state space is,

$$\begin{bmatrix} \dot{z}_1 \\ \dot{z}_2 \end{bmatrix} = \underbrace{\begin{bmatrix} 0 & 1 \\ 0 & 0 \end{bmatrix}}_A \begin{bmatrix} z_1 \\ z_2 \end{bmatrix} + \underbrace{\begin{bmatrix} 0 \\ \frac{1}{M} \end{bmatrix}}_B v \quad . \quad (3.60)$$

The closed loop poles are placed in $p = [-1 - 2]$ using matlab `place()`-command to obtain linear feedback gains, $\mathbf{k}_1 = [10.5460 \ 15.8190]$, resulting in the controller,

$$v = -\mathbf{k}_1 \mathbf{z} \quad , \quad (3.61)$$

where $\mathbf{z} = [x \ \dot{x}]^T$, such that,

$$v(x_2, x_4) = -\mathbf{k}_1 [x_2 \ x_4]^T \quad , \quad (3.62)$$

in terms of the full system. This control is added to the sat-based design and simulations are run without changing any previously designed gains.

Figure 3.17 shows the energy error reaching zero, taking one second longer under the influence of the linear controller, compared to Figure 3.12.

Chapter 3. Swing-Up Design

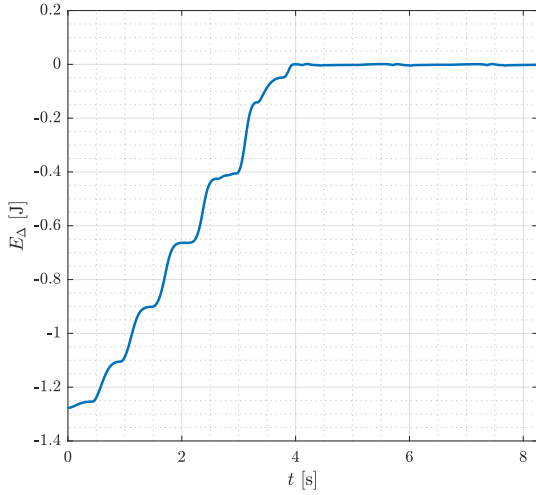


Figure 3.17: The sat-based controller reaches the reference in about four seconds, compared to three seconds it took without position and velocity control.

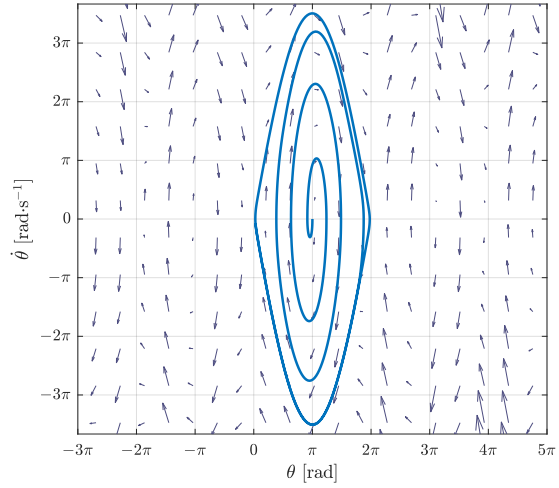


Figure 3.18: Though the sat-based energy controller reaches its reference one second slower when kept around $x = 0$, it still reaches the heteroclinic orbit with no overshoot.

In the phase portrait, see Figure 3.18, it is clear that the sat-based controller still reaches the heteroclinic orbit. Figure 3.19 shows how the linear control of the cart position and velocity successfully keeps the system within the available operating region of the real system.

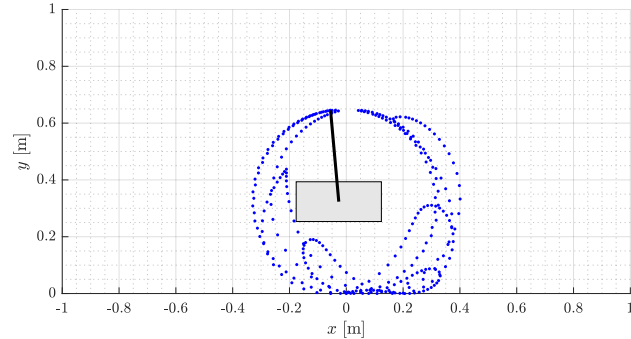


Figure 3.19: The linear control successfully keeps the cart around zero while the energy control approaches the unstable equilibrium.

Figure 3.20 shows the actuation required, the RMS is lower than it was before the linear controller was added. This could be tuned more tightly, but is left as a margin for now, with the possibility of further tuning during implementation.

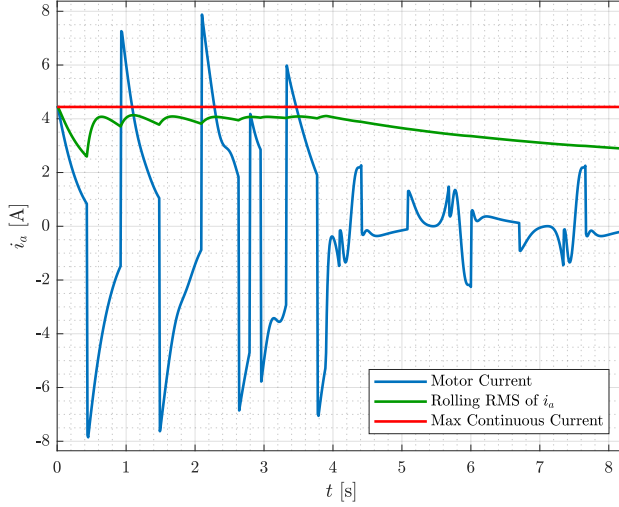


Figure 3.20: The control signal causes less continuous current, as seen by the lower RMS curve, this is left as a margin for now.

Figure 3.21 show the position approaching zero as the energy control settles, which is ideal, as it means the energy controller still has room to operate without fighting the linear feedback controller too much. Similarly, the oscillations around zero are necessary for the energy controller to keep its reference. Further, as seen in Figure 3.22 the velocity of the cart is also eventually controlled to zero by the added liner controller.

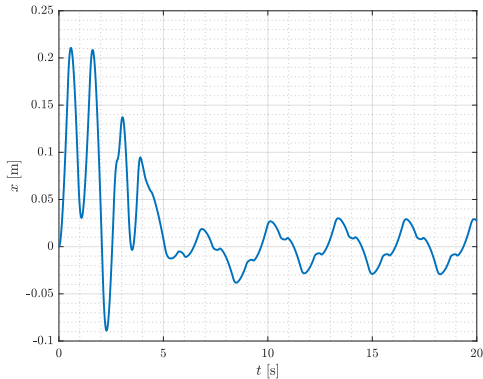


Figure 3.21: The saturation based controller keeps the cart closer to zero, suggesting less actuation from the energy control.

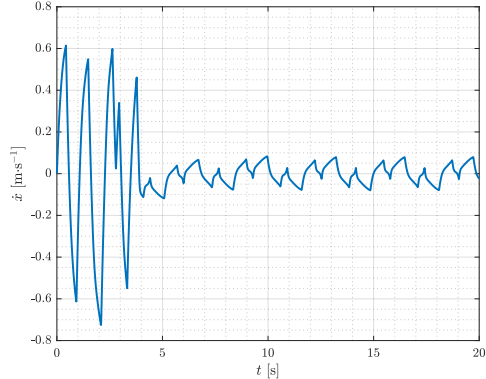


Figure 3.22: Zero velocity is obtained quite effectively after the energy reference is reached.

These two graphs are simulated over longer time to show that the linear controller reaches its reference.

This concludes the design of swing-up control.

4 | Stabilization

In this section the idea is to stabilize the pendulum in the unstable equilibrium. Ultimately this controller should be able to take over from the swing-up controller when some minimum catch angle is reached.

A sliding mode control strategy is employed to accomplish these goals. The design is based on [15].

Firstly, the model of the system, from Equation 2.15, is considered in following form,

$$\begin{bmatrix} \dot{x}_1 \\ \dot{x}_2 \\ \dot{x}_3 \\ \dot{x}_4 \end{bmatrix} = \underbrace{\begin{bmatrix} x_3 \\ x_4 \\ \mathbf{M}^{-1}(x_1)(-\mathbf{C}(x_1, x_3) - \mathbf{B}(x_3, x_4) - \mathbf{G}(x_1)) \end{bmatrix}}_{\mathbf{f}(\mathbf{x})} + \underbrace{\begin{bmatrix} 0 \\ 0 \\ \mathbf{M}^{-1}(x_1)\mathbf{F} \end{bmatrix}}_{\mathbf{g}(\mathbf{x})u}, \quad (4.1)$$

where,

$$\mathbf{M}^{-1} = \begin{bmatrix} \frac{(M+m)}{l^2m(M+m-m\cos^2 x_1)} & \frac{\cos x_1}{l(M+m-m\cos^2 x_1)} \\ \frac{\cos x_1}{l(M+m-m\cos^2 x_1)} & \frac{1}{M+m-m\cos^2 x_1} \end{bmatrix}, \quad (4.2)$$

with states $[x_1 \ x_2 \ x_3 \ x_4]^T = [\theta \ x \ \dot{\theta} \ \dot{x}]^T$ and input vector $\mathbf{F} = [0 \ u]^T$ as before.

In Equation 4.1 the input, u , appear in two of the four state equations. To design a sliding mode controller for the system, it is transformed into *regular form*,

$$\begin{aligned} \dot{\boldsymbol{\eta}} &= \mathbf{f}_a(\boldsymbol{\eta}, \xi) \\ \dot{\xi} &= f_b(\boldsymbol{\eta}, \xi) + g_b(\boldsymbol{\eta}, \xi)u \end{aligned}, \quad (4.3)$$

where the input only appears on one state equation. The transform is then given by,

$$\mathbf{T}(\mathbf{x}) = \begin{bmatrix} \boldsymbol{\eta} \\ \xi \end{bmatrix} \Rightarrow \frac{\partial}{\partial t} \mathbf{T}(\mathbf{x}) = \begin{bmatrix} \dot{\boldsymbol{\eta}} \\ \dot{\xi} \end{bmatrix} \Rightarrow \frac{\partial}{\partial t} \mathbf{T}(\mathbf{x}) = \begin{bmatrix} \mathbf{f}_a(\boldsymbol{\eta}, \xi) \\ f_b(\boldsymbol{\eta}, \xi) + g_b(\boldsymbol{\eta}, \xi)u \end{bmatrix}, \quad (4.4)$$

further,

$$\frac{\partial \mathbf{T}}{\partial t} = \frac{\partial \mathbf{T}}{\partial \mathbf{x}} \dot{\mathbf{x}} \quad (4.5)$$

$$\begin{bmatrix} \mathbf{f}_a(\boldsymbol{\eta}, \xi) \\ f_b(\boldsymbol{\eta}, \xi) + g_b(\boldsymbol{\eta}, \xi)u \end{bmatrix} = \frac{\partial \mathbf{T}}{\partial \mathbf{x}} \mathbf{f}(\mathbf{x}) + \frac{\partial \mathbf{T}}{\partial \mathbf{x}} \mathbf{g}(\mathbf{x})u, \quad (4.6)$$

such that,

$$\frac{\partial \mathbf{T}}{\partial \mathbf{x}} \mathbf{f}(\mathbf{x}) = \begin{bmatrix} \mathbf{f}_a(\boldsymbol{\eta}, \xi) \\ f_b(\boldsymbol{\eta}, \xi) \end{bmatrix} , \quad \frac{\partial \mathbf{T}}{\partial \mathbf{x}} \mathbf{g}(\mathbf{x}) = \begin{bmatrix} \mathbf{0} \\ g_b(\boldsymbol{\eta}, \xi) \end{bmatrix} . \quad (4.7)$$

Equation 4.7 results in the following four equations,

$$\begin{aligned} \frac{\partial \eta_1}{\partial x_3} g_3 + \frac{\partial \eta_1}{\partial x_4} g_4 &= 0 & \frac{\partial \eta_2}{\partial x_3} g_3 + \frac{\partial \eta_2}{\partial x_4} g_4 &= 0 \\ \frac{\partial \eta_3}{\partial x_3} g_3 + \frac{\partial \eta_3}{\partial x_4} g_4 &= 0 & \frac{\partial \xi}{\partial x_3} g_3 + \frac{\partial \xi}{\partial x_4} g_4 &= g_b(\boldsymbol{\eta}, \xi) \end{aligned} , \quad (4.8)$$

where,

$$\begin{bmatrix} g_3 \\ g_4 \end{bmatrix} u = \mathbf{M}^{-1}(x_1) \begin{bmatrix} 0 \\ u \end{bmatrix} \Rightarrow \begin{cases} g_3 = \frac{\cos x_1}{l(M+m-m \cos^2 x_1)} \\ g_4 = \frac{1}{M+m-m \cos^2 x_1} \end{cases} . \quad (4.9)$$

The following choice of coordinates to satisfy Equation 4.8 without loss of rank in \mathbf{T} , is based on the transform used for input-output linearization in [15].

Choosing output, $h(x) = \theta$ or $h(x) = x$, both results in the relative degree, $\rho = 2$, since the output appears on the second derivatives,

$$\ddot{\theta} = \dot{x}_3 = f_3 + g_3 u \quad (4.10)$$

$$\ddot{x} = \dot{x}_4 = f_4 + g_4 u . \quad (4.11)$$

The suggested transform is then,

$$\mathbf{T}(\mathbf{x}) = \begin{bmatrix} \phi_1(\mathbf{x}) \\ \vdots \\ \phi_{n-\rho}(\mathbf{x}) \\ h(\mathbf{x}) \\ L_f h(\mathbf{x}) \\ \vdots \\ L_f^{\rho-1} h(\mathbf{x}) \end{bmatrix} \Rightarrow \begin{bmatrix} \eta_1 \\ \eta_2 \\ \eta_3 \\ \xi \end{bmatrix} = \begin{bmatrix} \phi_1(\mathbf{x}) \\ \phi_2(\mathbf{x}) \\ h(\mathbf{x}) \\ L_f h(\mathbf{x}) \end{bmatrix} , \quad (4.12)$$

where $L_f h(\mathbf{x})$ is the *Lie derivative* of $h(\mathbf{x})$ along $f(\mathbf{x})$. This results in two possible transforms,

$$h = \theta \Rightarrow \mathbf{T}_1 = \begin{bmatrix} \eta_1 \\ \eta_2 \\ \eta_3 \\ \xi \end{bmatrix} = \begin{bmatrix} \phi_1 \\ \phi_2 \\ x_1 \\ x_3 \end{bmatrix} \quad \text{and} \quad h = x \Rightarrow \mathbf{T}_2 = \begin{bmatrix} \eta_1 \\ \eta_2 \\ \eta_3 \\ \xi \end{bmatrix} = \begin{bmatrix} \phi_1 \\ \phi_2 \\ x_2 \\ x_4 \end{bmatrix} , \quad (4.13)$$

leaving ϕ_1 and ϕ_2 to be determined. This is done by satisfying,

$$\frac{\partial \eta_1}{\partial x_3} g_3 + \frac{\partial \eta_1}{\partial x_4} g_4 = 0 \quad (4.14)$$

$$\frac{\partial \eta_2}{\partial x_3} g_3 + \frac{\partial \eta_2}{\partial x_4} g_4 = 0 \quad , \quad (4.15)$$

from Equation 4.8. For \mathbf{T}_1 the choice $\phi_1 = x_2$ satisfies Equation 4.14 with no loss of rank in the transform. Conversely for \mathbf{T}_2 the choice $\phi_1 = x_1$ satisfies Equation 4.14 again with no loss of rank. This leaves ϕ_2 which, for both transforms, is determined by finding a solution to Equation 4.15,

$$\frac{\partial \eta_2}{\partial x_3} \frac{\cos x_1}{l(M + m - m \cos^2 x_1)} + \frac{\partial \eta_2}{\partial x_4} \frac{1}{M + m - m \cos^2 x_1} = 0 \quad , \quad (4.16)$$

choosing,

$$\frac{\partial \eta_2}{\partial x_4} = \frac{\cos x_1}{l} \quad , \quad \frac{\partial \eta_2}{\partial x_3} = -1 \quad , \quad (4.17)$$

such that,

$$\eta_2 = \frac{\cos x_1}{l} x_4 - x_3 \quad . \quad (4.18)$$

This results in the following two transform candidates,

$$\mathbf{T}_1 = \begin{bmatrix} x_2 \\ \frac{\cos x_1}{l} x_4 - x_3 \\ x_1 \\ x_3 \end{bmatrix} \quad , \quad \mathbf{T}_2 = \begin{bmatrix} x_1 \\ \frac{\cos x_1}{l} x_4 - x_3 \\ x_2 \\ x_4 \end{bmatrix} \quad . \quad (4.19)$$

It is desired for the transform, \mathbf{T} , to be continuously differentiable and have a continuously differentiable inverse, \mathbf{T}^{-1} . Such a transform is known as a diffeomorphism. Further, \mathbf{T} is a global diffeomorphism iff its Jacobian is nonsingular for all $\mathbf{x} \in \mathbb{R}^n$ and $\lim_{\|\mathbf{x}\| \rightarrow \infty} \|\mathbf{T}(\mathbf{x})\| = \infty$, [15].

Thus the Jacobian of each transform is computed,

$$\mathbf{J}_1 = \frac{\partial \mathbf{T}_1(\mathbf{x})}{\partial \mathbf{x}} = \begin{bmatrix} 0 & 1 & 0 & 0 \\ -\frac{\sin x_1}{l} x_4 & 0 & -1 & \frac{\cos x_1}{l} \\ 1 & 0 & 0 & 0 \\ 0 & 0 & 1 & 0 \end{bmatrix} \quad (4.20)$$

$$\mathbf{J}_2 = \frac{\partial \mathbf{T}_2(\mathbf{x})}{\partial \mathbf{x}} = \begin{bmatrix} 1 & 0 & 0 & 0 \\ -\frac{\sin x_1}{l} x_4 & 0 & -1 & \frac{\cos x_1}{l} \\ 0 & 1 & 0 & 0 \\ 0 & 0 & 0 & 1 \end{bmatrix} \quad . \quad (4.21)$$

To check for singularity the determinant is found for the two Jacobian matrices,

$$\det(\mathbf{J}_1) = -\frac{\cos x_1}{l} \quad , \quad \det(\mathbf{J}_2) = 1 \quad . \quad (4.22)$$

If $\cos x_1 = 0$ the Jacobian, \mathbf{J}_1 , becomes singular. This only happens when the pendulum is in a horizontal position, which is outside the operating range of a stabilizing controller. However, the Jacobian, \mathbf{J}_2 , is nonsingular for all $\mathbf{x} \in \mathbb{R}^4$. Further, $\lim_{\|\mathbf{x}\| \rightarrow \infty} \|\mathbf{T}_2(\mathbf{x})\| = \infty$ so,

$$\mathbf{T} = \begin{bmatrix} \eta_1 \\ \eta_2 \\ \eta_3 \\ \xi \end{bmatrix} = \begin{bmatrix} x_1 \\ \frac{\cos x_1}{l} x_4 - x_3 \\ x_2 \\ x_4 \end{bmatrix} \quad , \quad (4.23)$$

is a global diffeomorphism and therefore chosen as the final system transform, with the inverse given by,

$$\mathbf{T}^{-1} = \begin{bmatrix} x_1 \\ x_2 \\ x_3 \\ x_4 \end{bmatrix} = \begin{bmatrix} \eta_1 \\ \eta_3 \\ \frac{\cos \eta_1}{l} \xi - \eta_2 \\ \xi \end{bmatrix} \quad . \quad (4.24)$$

The derivative of the transform, Equation 4.23, along the trajectories of the system is,

$$\begin{bmatrix} \dot{\eta}_1 \\ \dot{\eta}_2 \\ \dot{\eta}_3 \\ \dot{\xi} \end{bmatrix} = \begin{bmatrix} \dot{x}_1 \\ \frac{-\sin x_1}{l} \dot{x}_1 x_4 + \frac{\cos x_1}{l} \dot{x}_4 - \dot{x}_3 \\ \dot{x}_2 \\ \dot{x}_4 \end{bmatrix} \quad (4.25)$$

$$\begin{bmatrix} \dot{\eta}_1 \\ \dot{\eta}_2 \\ \dot{\eta}_3 \\ \dot{\xi} \end{bmatrix} = \begin{bmatrix} x_3 \\ \frac{-\sin x_1}{l} x_3 x_4 + \frac{\cos x_1}{l} f_4(\mathbf{x}) + \frac{\cos x_1}{l} g_4(\mathbf{x}) u - f_3(\mathbf{x}) - g_3(\mathbf{x}) u \\ x_4 \\ f_4(\mathbf{x}) + g_4(\mathbf{x}) u \end{bmatrix} \quad , \quad (4.26)$$

from which the *regular form* is obtained by rearranging and using the inverse transform,

$$\begin{bmatrix} \dot{\eta}_1 \\ \dot{\eta}_2 \\ \dot{\eta}_3 \\ \dot{\xi} \end{bmatrix} = \underbrace{\begin{bmatrix} \frac{\cos \eta_1}{l} \xi - \eta_2 \\ \frac{-\sin \eta_1}{l} (\frac{\cos \eta_1}{l} \xi - \eta_2) \xi + \frac{\cos \eta_1}{l} f_4(\boldsymbol{\eta}, \xi) - f_3(\boldsymbol{\eta}, \xi) \\ \xi \\ f_4(\boldsymbol{\eta}, \xi) \end{bmatrix}}_{f_a} + \underbrace{\begin{bmatrix} 0 \\ 0 \\ 0 \\ g_4(\boldsymbol{\eta}, \xi) \end{bmatrix}}_{g_b} u , \quad (4.27)$$

where,¹

$$\begin{aligned} f_3(\boldsymbol{\eta}, \xi) &= \frac{1}{l^2 m (M + m - m \cos^2 \eta_1)} \left[(M + m) b_{p,v} \left(\eta_2 - \frac{\cos \eta_1 \xi}{l} \right) + \right. \\ &\quad + (M + m) b_{p,c} \tanh \left(k_{\tanh} \left(\eta_2 - \frac{\cos \eta_1 \xi}{l} \right) \right) + m^2 g l \sin \eta_1 - b_{c,c} m l \tanh(k_{\tanh} \xi) \cos \eta_1 - \\ &\quad \left. - m^2 l^2 \cos \eta_1 \sin \eta_1 \left(\eta_2 - \frac{\xi \cos \eta_1}{l} \right)^2 + M g l m \sin \eta_1 - b_{c,v} m l \xi \cos \eta_1 \right] \end{aligned} \quad (4.28)$$

$$\begin{aligned} f_4(\boldsymbol{\eta}, \xi) &= -\frac{1}{l (M + m - m \cos^2 \eta_1)} \left[b_{c,v} l \xi - b_{p,v} \cos \eta_1 \left(\eta_2 - \frac{\cos \eta_1 \xi}{l} \right) + b_{c,c} l \tanh(k_{\tanh} \xi) - \right. \\ &\quad - b_{p,c} \tanh \left(k_{\tanh} \left(\eta_2 - \frac{\cos \eta_1 \xi}{l} \right) \right) \cos \eta_1 + \\ &\quad \left. + l^2 m \sin \eta_1 \left(\eta_2 - \frac{\xi \cos \eta_1}{l} \right)^2 - m g l \cos \eta_1 \sin \eta_1 \right] \end{aligned} \quad (4.29)$$

$$g_4(\boldsymbol{\eta}, \xi) = \frac{1}{M + m - m \cos^2 \eta_1} . \quad (4.30)$$

With the system on regular form, design is proceeded by choosing a sliding manifold,

$$s = \xi - \phi(\boldsymbol{\eta}) , \quad (4.31)$$

where $\phi(\boldsymbol{\eta})$ is to be designed. If s is zero then $\xi = \phi(\boldsymbol{\eta})$, such that,

$$\dot{\boldsymbol{\eta}} = f_a(\boldsymbol{\eta}, \phi(\boldsymbol{\eta})) , \quad (4.32)$$

is the reduced-order system with $\phi(\boldsymbol{\eta})$ as control input. It is then sought to design $\phi(\boldsymbol{\eta})$ such that Equation 4.32 is asymptotically stable at its origin.

To that end, the reduced-order system is linearized,

$$A = \frac{\partial \dot{\boldsymbol{\eta}}}{\partial \boldsymbol{\eta}} \Bigg|_{\substack{\boldsymbol{\eta}=\mathbf{0} \\ \xi=0 \\ k_{\tanh}=1}} = \begin{bmatrix} 0 & -1 & 0 \\ -\frac{g}{l} & \frac{-b_{p,v}}{l^2 m} & 0 \\ 0 & 0 & 0 \end{bmatrix} , \quad B = \frac{\partial \dot{\boldsymbol{\eta}}}{\partial \xi} \Bigg|_{\substack{\boldsymbol{\eta}=\mathbf{0} \\ \xi=0 \\ k_{\tanh}=1}} = \begin{bmatrix} \frac{1}{l} \\ \frac{b_{p,v}+b_{p,c}l}{l^3 m} \\ 1 \end{bmatrix} . \quad (4.33)$$

¹FiXme Note: Is this too much?

Checking for controllability,

$$\text{rank}(\mathcal{C}) = \text{rank}([B \ AB \ A^2B]) = 3 \quad , \quad (4.34)$$

and since the controllability matrix, \mathcal{C} , has full rank, the linearized system is controllable. A state feedback controller is designed for the linearized reduced-order system,

$$\phi(\boldsymbol{\eta}) = -\mathbf{k}\boldsymbol{\eta} \quad . \quad (4.35)$$

The poles are placed in $\mathbf{p} = [-4 \ -5 \ -6]$ using matlab *place()*-command to obtain the gains, $\mathbf{k} = [4.5824 \ -0.8341 \ -1.9766]$. Simulations of the controlled reduced-order system are run for both the linearized and the nonlinear system, see Figure 4.1.

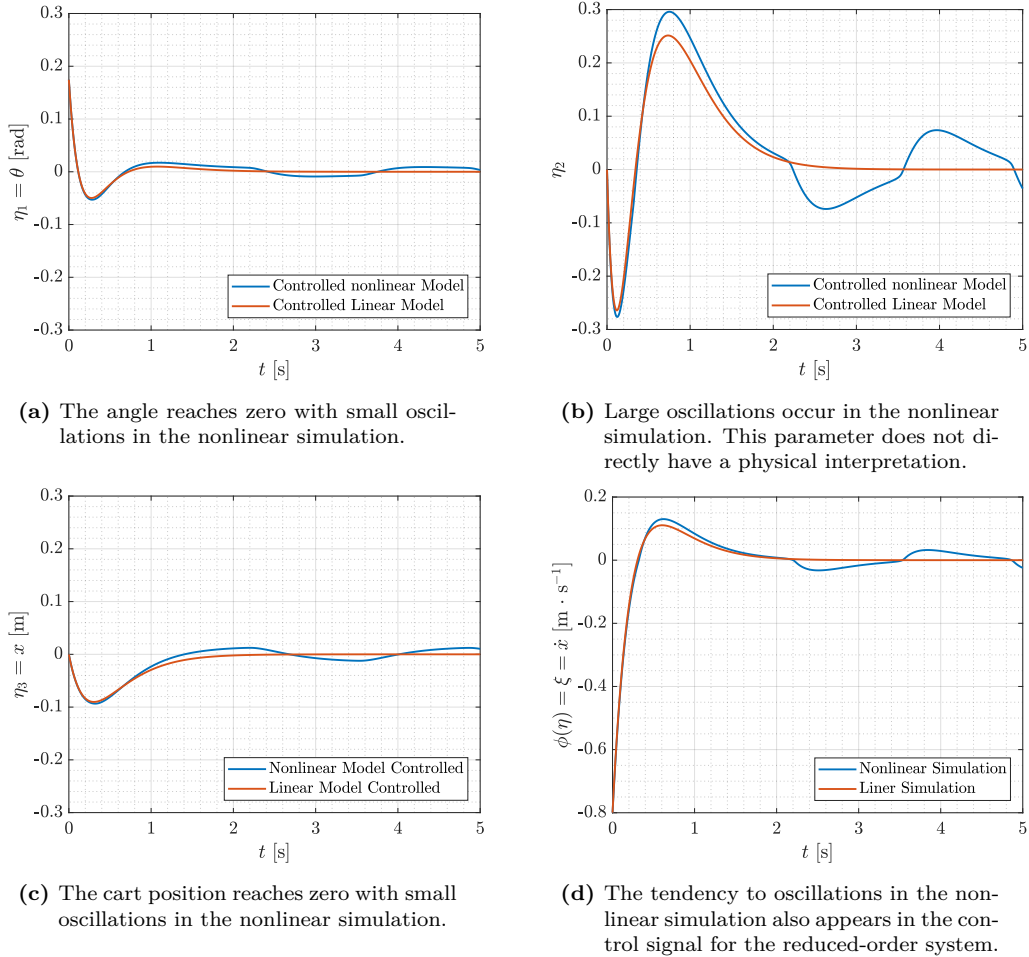


Figure 4.1: Nonlinear and linear simulation of the state feedback control designed for the linearized reduced-order system.

The reduced-order system is stabilized under the assumption that s is zero. Thus, the design of u is concerned with bringing s to zero.

Theorem 4.0.1 (Lyapunov Stability Theorem) Consider the autonomous system, $f(\mathbf{x}) = \dot{\mathbf{x}}$, where $f : \mathbb{D} \rightarrow \mathbb{R}^n$ is locally Lipschitz and $\mathbf{x} = \mathbf{0}$ is an equilibrium point. Then if $\exists V : \mathbb{D} \rightarrow \mathbb{R}$ and

1. $V(\mathbf{x})$ is C^1
2. $V(\mathbf{x}) > 0 \forall \mathbf{x} \in \mathbb{D} \setminus \{0\}$ and $V(\mathbf{0}) = 0$
3. $\dot{V}(\mathbf{x}) \leq 0$ in \mathbb{D}

then $\mathbf{x} = \mathbf{0}$ is stable. Further, if,

$$\dot{V}(\mathbf{x}) < 0 \text{ in } \mathbb{D} \setminus \{0\} ,$$

then $\mathbf{x} = \mathbf{0}$ is asymptotically stable [15].

A Lyapunov function candidate is proposed,

$$V(\boldsymbol{\eta}, \xi) = \frac{1}{2}s^2 , \quad (4.36)$$

where $s = \xi - \mathbf{k}\boldsymbol{\eta}$ hence,

$$V = \frac{1}{2}(\xi - \mathbf{k}\boldsymbol{\eta})^2 \quad (4.37)$$

$$V = \frac{1}{2}(\xi^2 + (\mathbf{k}\boldsymbol{\eta})^2) - \xi\mathbf{k}\boldsymbol{\eta} \quad (4.38)$$

$$V = \frac{1}{2}(\xi^2 + k_1^2\eta_1^2 + k_2^2\eta_2^2 + k_3^2\eta_3^2) + k_1k_2\eta_1\eta_2 + k_1k_3\eta_1\eta_3 + k_2k_3\eta_2\eta_3 - \xi(k_1\eta_1 + k_2\eta_2 + k_3\eta_3) . \quad (4.39)$$

The partial derivatives are,

$$\frac{\partial V}{\partial \xi} = \xi - \mathbf{k}\boldsymbol{\eta} \quad (4.40)$$

$$\frac{\partial V}{\partial \eta_1} = k_1^2\eta_1 + k_1k_2\eta_2 + k_1k_3\eta_3 - k_1\xi , \quad (4.41)$$

and similar results to Equation 4.41 are obtained for the partial derivatives with respect to η_2 and η_3 . Since all four partial derivatives are C^0 then V is C^1 in the entire \mathbb{R}^4 , thus satisfying the first condition of the Lyapunov Stability Theorem 4.0.1. Further, from Equation 4.37, it is clear that V is positive definite in the entire state space without zero and zero in the origin, thus also satisfying the second condition.

To assess the third condition of Theorem 4.0.1, the derivative of the Lyapunov function candidate is found along trajectories of the system,

$$\dot{V} = s\dot{s} \quad (4.42)$$

$$\dot{V} = s(\dot{\xi} + \mathbf{k}\dot{\boldsymbol{\eta}}) \quad (4.43)$$

$$\dot{V} = s(f_b(\boldsymbol{\eta}, \xi) + g_b(\boldsymbol{\eta}, \xi)u + \mathbf{k}f_a(\boldsymbol{\eta}, \xi)) \quad (4.44)$$

$$\dot{V} = (\mathbf{k}f_a + f_b)s + g_bsu \quad (4.45)$$

$$\dot{V} = g_bs(\mathbf{k}f_a + f_b)g_b^{-1} + g_bsu \quad (4.46)$$

$$\dot{V} \leq g_b|s| |\mathbf{k}f_a + f_b| g_b^{-1} + g_bsu . \quad (4.47)$$

This leads to the design of u which is chosen such that the third condition of Theorem 4.0.1 is satisfied,

$$u = -\text{sgn}(s)\beta(\boldsymbol{\eta}, \xi)g_b^{-1}(\boldsymbol{\eta}, \xi) \quad \text{where,} \quad \beta(\boldsymbol{\eta}, \xi) = \varrho(\boldsymbol{\eta}, \xi) + \beta_0 \quad (4.48)$$

$$\varrho(\boldsymbol{\eta}, \xi) = |\mathbf{k}f_a + f_b| \quad , \quad (4.49)$$

and $\beta_0 > 0$ is a tuning parameter allowing \dot{V} to be positive definite, thereby guaranteeing asymptotic stability of the origin by Theorem 4.0.1,

$$\dot{V} < g_b|s| |\mathbf{k}f_a + f_b| g_b^{-1} - g_b \text{sgn}(s)s |\mathbf{k}f_a + f_b + \beta_0| g_b^{-1} \quad . \quad (4.50)$$

For implementation, the discontinuity introduced by the sign-function in the control law is cause for excessive switching and chattering due to delays in the real system. To circumvent this issue, a saturation function with a steep slope, $1/\varepsilon$, is used to approximate the sign-function,

$$\text{sat}(s/\varepsilon) = \begin{cases} s/\varepsilon & |s/\varepsilon| \leq 1 \\ \text{sgn}(s) & |s/\varepsilon| > 1 \end{cases} , \quad (4.51)$$

hence,

$$u = -\text{sat}(s/\varepsilon)\beta(\boldsymbol{\eta}, \xi)g_b^{-1}(\boldsymbol{\eta}, \xi) \quad . \quad (4.52)$$

Part II

Twin Pendulum

5 | System and Model

The cart pendulum system from *Part 1* is used again. However, here in *Part 2* an additional pendulum is mounted on the cart. The modification is discussed and a model for the changed system is developed in this chapter. The remaining of *Part 2* is concerned with estimating parameters, developing a state estimator and ultimately stabilizing the two pendulums in upright position.

5.1 System Addition

5.2 Model

To model the twin pendulum system, consider the excessive coordinate convention in Figure 5.1 along with the generalized coordinates in the mechanical drawing, Figure 5.2.

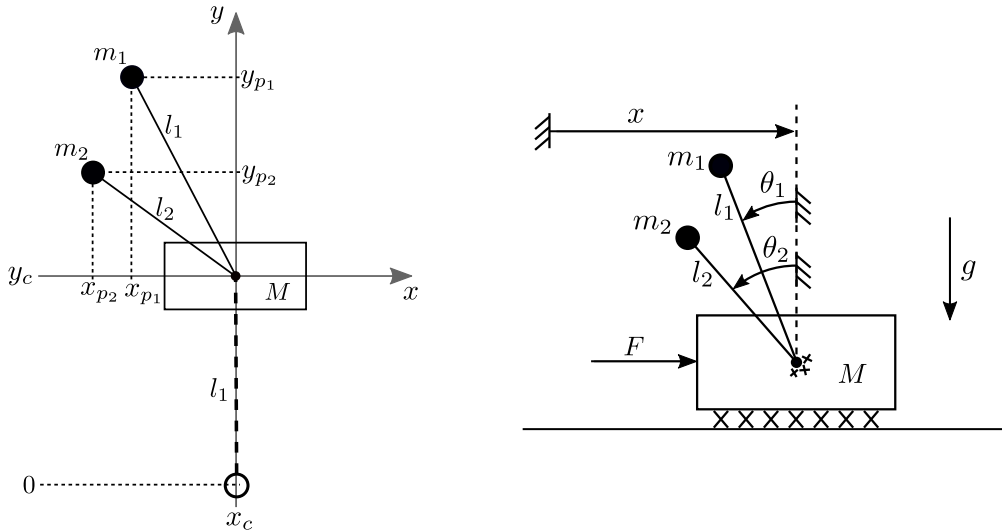


Figure 5.1: Twin pendulum system in excessive coordinates.

Figure 5.2: Mechanical drawing of the system with the added pendulum in generalized coordinates.

The energy method is applied. First the potential and kinetic energies, in terms of excessive coordinates, is found,

$$U = Mg y_c + m_1 g y_{p1} + m_2 g y_{p2} \quad (5.1)$$

$$T = \frac{1}{2} M \dot{x}_c^2 + \frac{1}{2} M \dot{y}_c^2 + \frac{1}{2} m_1 \dot{x}_{p1}^2 + \frac{1}{2} m_1 \dot{y}_{p1}^2 + \frac{1}{2} m_2 \dot{x}_{p2}^2 + \frac{1}{2} m_2 \dot{y}_{p2}^2 . \quad (5.2)$$

The excessive coordinates and derivatives thereof are then expressed in terms of the

generalized coordinates, using the conventions presented in Figure 5.1 and 5.2,

$$\begin{cases} x_c = x \\ y_c = l_1 \end{cases} \quad \begin{cases} x_{p_1} = x - l_1 \sin \theta_1 \\ y_{p_1} = l_1 + l_1 \cos \theta_1 \end{cases} \quad \begin{cases} x_{p_2} = x - l_2 \sin \theta_2 \\ y_{p_2} = l_1 + l_2 \cos \theta_2 \end{cases} \quad (5.3)$$

$$\begin{cases} \dot{x}_c = \dot{x} \\ \dot{y}_c = 0 \end{cases} \quad \begin{cases} \dot{x}_{p_1} = \dot{x} - l_1 \sin \theta_1 \\ \dot{y}_{p_1} = -l_1 \sin \theta_1 \dot{\theta}_1 \end{cases} \quad \begin{cases} \dot{x}_{p_2} = \dot{x} - l_2 \sin \theta_2 \\ \dot{y}_{p_2} = -l_2 \sin \theta_2 \dot{\theta}_2 \end{cases} \quad . \quad (5.4)$$

Inserting Equation 5.3 and 5.4 into the energy equations, Equation 5.1 and 5.2, yields,

$$U = Mgl_1 + m_1g(l_1 + l_1 \cos \theta_1) + m_2g(l_1 + l_2 \cos \theta_2) \quad (5.5)$$

$$T = \frac{1}{2}M\dot{x}^2 + \frac{1}{2}m_1(\dot{x} - l_1 \sin \theta_1)^2 + \frac{1}{2}m_1(-l_1 \sin \theta_1 \dot{\theta}_1)^2 + \frac{1}{2}m_2(\dot{x} - l_2 \sin \theta_2)^2 + \frac{1}{2}m_2(-l_2 \sin \theta_2 \dot{\theta}_2)^2 \quad . \quad (5.6)$$

Proceeding to compute the Lagrangian,

$$\mathcal{L} = T - U \quad (5.7)$$

$$\begin{aligned} \mathcal{L} = & \frac{1}{2}M\dot{x}^2 + \frac{1}{2}m_1(\dot{x}^2 + l_1^2 \cos^2 \theta_1 \dot{\theta}_1^2 - 2\dot{x}l_1 \cos \theta_1 \dot{\theta}_1) + \frac{1}{2}m_1l_1^2 \sin^2 \theta_1 \dot{\theta}_1^2 + \\ & + \frac{1}{2}m_2(\dot{x}^2 + l_2^2 \cos^2 \theta_2 \dot{\theta}_2^2 - 2\dot{x}l_2 \cos \theta_2 \dot{\theta}_2) + \frac{1}{2}m_2l_2^2 \sin^2 \theta_2 \dot{\theta}_2^2 - \\ & - (M + m_1 + m_2)gl_1 - m_1gl_1 \cos \theta_1 - m_2gl_2 \cos \theta_2 \end{aligned} \quad (5.8)$$

$$\begin{aligned} \mathcal{L} = & \frac{1}{2}(M + m_1 + m_2)\dot{x}^2 - (m_1l_1 \cos \theta_1 \dot{\theta}_1 + m_2l_2 \cos \theta_2 \dot{\theta}_2)\dot{x} + \\ & + \frac{1}{2}m_1l_1^2(\cos^2 \theta_1 + \sin^2 \theta_1)\dot{\theta}_1^2 + \frac{1}{2}m_2l_2^2(\cos^2 \theta_2 + \sin^2 \theta_2)\dot{\theta}_2^2 - \\ & - (M + m_1 + m_2)gl_1 - m_1gl_1 \cos \theta_1 - m_2gl_2 \cos \theta_2 \end{aligned} \quad (5.9)$$

$$\begin{aligned} \mathcal{L} = & \frac{1}{2}(M + m_1 + m_2)\dot{x}^2 - (m_1l_1 \cos \theta_1 \dot{\theta}_1 + m_2l_2 \cos \theta_2 \dot{\theta}_2)\dot{x} + \frac{1}{2}m_1l_1^2\dot{\theta}_1^2 + \\ & + \frac{1}{2}m_2l_2^2\dot{\theta}_2^2 - (M + m_1 + m_2)gl_1 - m_1gl_1 \cos \theta_1 - m_2gl_2 \cos \theta_2 \quad , \end{aligned} \quad (5.10)$$

and finally by using the Lagrange-d'Alembert Principle, [9]

$$\frac{d}{dt} \frac{\partial \mathcal{L}}{\partial \dot{\mathbf{q}}} - \frac{\partial \mathcal{L}}{\partial \mathbf{q}} = \mathbf{Q} \quad , \quad (5.11)$$

$$\mathbf{q} = \begin{bmatrix} \theta_1 \\ \theta_2 \\ x \end{bmatrix} \quad , \quad \mathbf{Q} = \begin{bmatrix} -b_{p_1,v}\dot{\theta}_1 - \tanh(k_{\tanh}\dot{\theta}_1)b_{p_1,c} \\ -b_{p_2,v}\dot{\theta}_2 - \tanh(k_{\tanh}\dot{\theta}_2)b_{p_2,c} \\ u - b_{c,v}\dot{x} - \tanh(k_{\tanh}\dot{x})b_{c,c} \end{bmatrix} \quad . \quad (5.12)$$

Note that, as in *Part 1*, the control output is seen as the force on the cart directly, $u = F$, to avoid excessive notation. Equation 5.11 is computed for each generalized coordinate starting with the first pendulum angle, θ_1 ,

$$\frac{d}{dt} \frac{\partial \mathcal{L}}{\partial \dot{\theta}_1} - \frac{\partial \mathcal{L}}{\partial \theta_1} = Q_1 \quad (5.13)$$

$$m_1l_1 \sin \theta_1 \dot{\theta}_1 \dot{x} - m_1l_1 \cos \theta_1 \ddot{x} + m_1l_1^2 \dot{\theta}_1^2 - m_1l_1 \sin \theta_1 \dot{\theta}_1 \dot{x} - m_1gl_1 \sin \theta_1 = Q_1 \quad (5.14)$$

$$-m_1l_1 \cos \theta_1 \dot{x} + m_1l_1^2 \ddot{\theta}_1 - m_1gl_1 \sin \theta_1 = -b_{p_1,v}\dot{\theta}_1 - \tanh(k_{\tanh}\dot{\theta}_1)b_{p_1,c} \quad , \quad (5.15)$$

similarly for the second pendulum angle, θ_2 ,

$$-m_2 l_2 \cos \theta_2 \ddot{x} + m_2 l_2^2 \ddot{\theta}_2 - m_2 g l_2 \sin \theta_2 = -b_{p_2,v} \dot{\theta}_2 - \tanh(k_{\tanh} \dot{\theta}_2) b_{p_2,c} , \quad (5.16)$$

and finally for the cart position, x ,

$$\frac{d}{dt} \frac{\partial \mathcal{L}}{\partial \dot{x}} - \frac{\partial \mathcal{L}}{\partial x} = Q_3 \quad (5.17)$$

$$(M + m_1 + m_2) \ddot{x} + m_1 l_1 \sin \theta_1 \dot{\theta}_1^2 - m_1 l_1 \cos \theta_1 \ddot{\theta}_1 + \\ + m_2 l_2 \sin \theta_2 \dot{\theta}_2^2 - m_2 l_2 \cos \theta_2 \ddot{\theta}_2 = u - b_{c,v} \dot{x} - \tanh(k_{\tanh} \dot{x}) b_{c,c} . \quad (5.18)$$

The final dynamic equations for the twin pendulum system are then,

$$-m_1 l_1 \cos \theta_1 \ddot{x} + m_1 l_1^2 \ddot{\theta}_1 - m_1 g l_1 \sin \theta_1 = Q_1 \quad (5.19)$$

$$-m_2 l_2 \cos \theta_2 \ddot{x} + m_2 l_2^2 \ddot{\theta}_2 - m_2 g l_2 \sin \theta_2 = Q_2 \quad (5.20)$$

$$(M + m_1 + m_2) \ddot{x} + m_1 l_1 \sin \theta_1 \dot{\theta}_1^2 - m_1 l_1 \cos \theta_1 \ddot{\theta}_1 + m_2 l_2 \sin \theta_2 \dot{\theta}_2^2 - m_2 l_2 \cos \theta_2 \ddot{\theta}_2 = Q_3 , \quad (5.21)$$

and arranged in following manner,

$$\begin{bmatrix} m_1 l_1^2 & 0 & -m_1 l_1 \cos \theta_1 \\ 0 & m_2 l_2^2 & -m_2 l_2 \cos \theta_2 \\ -m_1 l_1 \cos \theta_1 & -m_2 l_2 \cos \theta_2 & M + m_1 + m_2 \end{bmatrix} \begin{bmatrix} \ddot{\theta}_1 \\ \ddot{\theta}_2 \\ \ddot{x} \end{bmatrix} + \begin{bmatrix} 0 \\ 0 \\ m_1 l_1 \sin \theta_1 \dot{\theta}_1^2 + m_2 l_2 \sin \theta_2 \dot{\theta}_2^2 \end{bmatrix} + \\ + \begin{bmatrix} -b_{p_1,v} \dot{\theta}_1 - \tanh(k_{\tanh} \dot{\theta}_1) b_{p_1,c} \\ -b_{p_2,v} \dot{\theta}_2 - \tanh(k_{\tanh} \dot{\theta}_2) b_{p_2,c} \\ -b_{c,v} \dot{x} - \tanh(k_{\tanh} \dot{x}) b_{c,c} \end{bmatrix} = \begin{bmatrix} 0 \\ 0 \\ u \end{bmatrix} , \quad (5.22)$$

the well known general form of an m-link robot is obtained, [12, 13]

$$\mathbf{M}(\mathbf{q}) \ddot{\mathbf{q}} + \mathbf{C}(\mathbf{q}, \dot{\mathbf{q}}) + \mathbf{B}(\dot{\mathbf{q}}) + \mathbf{G}(\mathbf{q}) = \mathbf{F} , \quad (5.23)$$

where,

$\mathbf{M}(\mathbf{q})$ is the inertia matrix

$\mathbf{C}(\mathbf{q}, \dot{\mathbf{q}})$ is the Coriolis and centrifugal effects

$\mathbf{B}(\dot{\mathbf{q}})$ is the friction

$\mathbf{G}(\mathbf{q})$ is the force due to gravity

\mathbf{F} is the input force vector .

Chapter 5. System and Model

Choosing states $[x_1 \ x_2 \ x_3 \ x_4 \ x_5 \ x_6]^T = [\theta_1 \ \theta_2 \ x \ \dot{\theta}_1 \ \dot{\theta}_2 \ \dot{x}]^T$ results in the nonlinear state space representation,

$$\begin{bmatrix} \dot{x}_1 \\ \dot{x}_2 \\ \dot{x}_3 \\ \dot{x}_4 \\ \dot{x}_5 \\ \dot{x}_6 \end{bmatrix} = \begin{bmatrix} x_4 \\ x_5 \\ x_6 \\ \mathbf{M}^{-1}(x_1, x_2)(\mathbf{F} - \mathbf{C}(x_1, x_2, x_4, x_5) - \mathbf{B}(x_4, x_5, x_6) - \mathbf{G}(x_1, x_2)) \end{bmatrix}. \quad (5.24)$$

Bibliography

- [1] *Maxon RE Motor*. Oct. 8, 2018. URL: https://www.maxonmotor.com/medias/sys_master/root/8825409470494/17-EN-133.pdf.
- [2] Avago Technologies. *HEDM-55xx/560x & HEDS-55xx/56xx*. Aug. 15, 2018. URL: https://www.infineon.com/dgdl/Infineon-Encoder_HEDS-5540-A14-AP-v01_00-EN.pdf?fileId=5546d46147a9c2e40147d3d593970357.
- [3] *Maxon Controller*. Aug. 15, 2018. URL: <https://www.maxonmotor.com/maxon/view/product/control/Servoerstaerker-4-Q-DC/201583>.
- [4] *sparkfun Teensy 3.6*. Aug. 15, 2018. URL: <https://www.sparkfun.com/products/14057>.
- [5] *HCTL-2021 PLC Avago Datasheet*. Aug. 15, 2018. URL: <https://datasheet.octopart.com/HCTL-2021-PLC-Avago-datasheet-7580518.pdf>.
- [6] *K66 Sub-Family Reference Manual*. Aug. 15, 2018. URL: <https://cdn.sparkfun.com/datasheets/Dev/Arduino/Boards/K66P144M180SF5RMV2.pdf>.
- [7] Jonas Ørndrup Jesper H. Hørgensen. *Non-linear Control and Machine Learning on an Inverted Pendulum on a Cart*. Master Thesis. 2018.
- [8] Niels Skov Vestergaard. *Sliding Mode Stabilization and Phase Plane Trajectory Planning for a Cart Pendulum System*. 9th Semester Project. 2018.
- [9] Rafael Wisniewski. *Mechanical Systems II. Lagrange Mechanics*. Aalborg University, 2013.
- [10] Charles M. Close, Dean K. Frederick, and Jonathan C. Newell. *Modeling and Analysis of Dynamic Systems*. Wiley, 2001.
- [11] H. Olsson et al. *Friction Models and Friction Compensation*. Nov. 28, 1997.
- [12] Mark W. Spong, Seth Hutchinson, and M. Vidyasagar. *Robot Dynamics and Control*. 2nd ed. Wiley, 2005.
- [13] Lorenzo Sciavicco and Bruno Siciliano. *Modelling and Control of Robot Manipulators*. 2nd ed. Lorenzo Sciavicco and Bruno Siciliano. London: Springer, 2012.
- [14] Karl Johan Åström and Katsuhisa Furuta. “Swinging up a pendulum by energy control”. In: *Automatica* 36.2 (2000), pp. 287–295.
- [15] Hassan K. Khalil. *Nonlinear Systems*. 3rd ed. 2015.

List of Corrections

Note: Is this too much? 27